Compact solid-state lasers in the near-infrared and visible spectral range

KAI SEGER

ROYAL INSTITUTE
OF TECHNOLOGY

Doctoral Thesis
Department of Applied Physics
KTH – Royal Institute of Technology
Stockholm, Sweden 2013

Compact solid-state lasers in the near-infrared and visible spectral range

Laser Physics
Department of Applied Physics
KTH – Royal Institute of Technology
106 91 Stockholm
Sweden

ISBN 978-91-7501-764-8
TRITA-FYS 2013:13
ISSN 0280-316X
ISRN KTH/FYS/–13:13-SE

Akademisk avhandling som med tillstånd av Kungliga Tekniska Högskolan framlägges till offentlig granskning för avläggande av teknologie doktorsexamen fredagen den 30 maj 2013 kl. 10.00 i sal FD5, Albanova, Roslagstullsbacken 21, KTH, Stockholm. Avhandlingen kommer att försvaras på engelska.

Printed by Universitetsservice US AB, Stockholm 2013

Kai Seger
Compact solid-state lasers in the near-infrared and visible spectral range
Laser Physics, Department of Applied Physics, KTH – Royal Institute of Technology, 106 91 Stockholm, Sweden
ISBN 978-91-7501-764-8, TRITA-FYS 2013:13, ISSN 0280-316X, ISRN KTH/FYS/–13:13-SE

Abstract

The subject of this thesis is the exploration of new concepts for compact solid-state lasers in the visible and near-infrared spectral range using new components such as volume Bragg gratings for wavelength stabilisation and wavelength tuning. Also single-walled carbon nanotubes for mode-locking and Q-switching of lasers have been studied.

We have developed a new method for the tuning of solid-state lasers by replacing a dielectric mirror with a transversally chirped volume Bragg grating, which allows smooth wavelength tuning without additional elements inside the laser cavity. The result is a more compact laser, since the tuning mechanism and output coupler are incorporated in one component. Another benefit is an increased efficiency, since additional elements inside the cavity will always add to the total loss of the laser. This has been demonstrated for a broadband ytterbium laser around 1 μm and a single-longitudinal-mode Nd:YVO_4 laser around 1.06 μm.
A volume Bragg grating has also been used to construct an efficient, narrow-linewidth ytterbium fiber laser and the employment of a volume Bragg grating as the pump mirror of a solid-state laser for frequency-doubling has been investigated. Both lasers represent a practical solution, eliminating the use of additional intracavity elements.
Second-harmonic generation is an efficient way to access the visible spectral range using diode-pumped solid-state lasers. However, these lasers can suffer from large amplitude fluctuations, which has been analyzed in more detail for an optically-pumped semiconductor disk-laser and a volume Bragg grating locked ytterbium laser. The control of those amplitude fluctuations is very important, since many applications like fluorescence microscopy require a laser with a constant output power and as little noise as possible.
In addition to this, we have demonstrated, that saturable absorbers based on quantum dots and carbon nanotubes can be used to mode-lock compact laser at a wavelength around 1.03 μm. Those lasers have many interesting applications in communications, clock generation, metrology and life sciences.

Sammanfattning

Ämnet för denna avhandling har varit att utforska nya koncept för kompakta fasta-tillståndslasrar i det synliga och nära infraröda spektralområdet. Ett antal nya komponenter har introducerats såsom volymbraggitter för stabilisering och avstämning av våglängden och enkelväggiga kolnanorör för modlåsning och Q-switchning av lasrarna.

Vi har utvecklat en ny metod för våglängdsavstämning av fasta-tillståndslasrar genom att ersätta en dielektrisk spegel med ett volymbraggitter. Gittret har en transversellt varierande gitterperiod, vilket möjliggör en smidig våglängdsavstämning genom att gittret förflyttas i sidled utan att något ytterligare komponent krävs i laserkaviten.
Resultatet är en mer kompakt avstämbar laser än vad som fanns tidigare, eftersom avstämnings-mekanismen och utkopplingspegeln är en och samma komponent. En annan fördel är att lasern blir effektivare, dåfärre komponenter minskar de totala förlusterna. Konceptet visade vi för en ytterbium-laser som var bredbandigt avstämbar vid vågländsområdet kring 1 μm och för en Nd:YVO_4 laser, vilken lasrade med en enda longitudinell mode vid 1.06 μm.
Ett volymbraggitter har också använts för att konstruera en effektiv, ytterbium-dopad fiber-laser med smalbandigt spektra. Vidare har vi undersökts om ett volymbraggitter kan användas som inkopplingsspegel för pumpen för en frekvensdubblad fasta-tillståndslaser. Båda lasrarna är praktiska lösningar, som minimerar antalet komponenter i laserkaviteten, samtidigt som det ger stabil och effektiv lasring vid en förutbestämd önskad våglängd.
Frekvensdubling är ett effektivt sätt att nå det synliga spektralområdet med diod-pumpade fasta-tillståndslasrar. Dessa lasrar har ofta kraftiga amplitudsvängningar, vilka vi har analyserat i detalj för en optiskt pumpade halvledardisklaser och en volymbraggitter låst ytterbium laser. Kontrollen av dessa amplitudsvängningar är mycket viktigt, eftersom många tillämpningar som t.ex. fluorescensmikroskopi kräver en laser med en konstant uteffekt och minimalt brus.
Slutligen har vi visat att mättningsbara absorbatorer baserade på kvantpricksstrukturer i halvledare och kolnanorördopade polymerfilmer kan användas för konstruera praktiska och kompakta modlåsta fasta-tillståndslaser vid en våglängd kring 1.03 μm. Dessa lasrar har många intressanta tillämpningar inom kommunikation, klockgenerering, metrologi och bioteknik.

Contents

List of publications

Publications included in the thesis

This thesis is based on the following journal papers:

I Kai Seger, Björn Jacobsson, Valdas Pasiskevicius and Fredrik Laurell
Tunable Yb:KYW laser using a transversely chirped volume Bragg grating
Optics Express **17**, 2341 (2009).

II Kai Seger, Niels Meiser, Carlota Canalias, Valdas Pasiskevicius and Fredrik Laurell
Tunable, passively Q-switched single-longitudinal-mode Nd:YVO_4 laser using a chirped volume Bragg grating
Applied Physics B **109**, 99 (2012).

III Pär Jelger, Kai Seger, Valdas Pasiskevicius and Fredrik Laurell
Highly efficient temporally stable narrow linewidth cryogenically cooled Yb-fiber laser
Optics Express **17**, 8433 (2009).

IV Niels Meiser, Kai Seger, Valdas Pasiskevicius, Hoon Jang, Edik Rafailov and Igor Krestnikov
GHz repetition rate mode-locked Yb:KYW laser using self-assembled quantum dot saturable absorber
Applied Physics B **110**, 327 (2013).

V Rene Hartke, Valery Baev, Kai Seger, Oliver Back, Ernst Heumann, Günter Huber, Michael Kühnelt, Ulrich Steegmüller
Experimental study of the output dynamics of intracavity frequency doubled OPSDL
Applied Physics Letters **92**, 101107 (2008).

VI Kai Seger, Niels Meiser, Staffan Tjörnhammar, andrius Zukauskas, Carlota Canalias, Valdas Pasiskevicius and Fredrik Laurell
Intra-cavity frequency-doubled Yb:KYW laser using periodically poled Rb-doped KTP with a volume Bragg grating input coupler
Submitted for publication (2013).

VII Kai Seger, Niels Meiser, Sun Young Choi, Bo Hee Jung, Dong-Il Yeom, Fabian Rotermund, Oleg Okhotnikov, Fredrik Laurell and Valdas Pasiskevicius
Carbon nanotube mode-locked optically-pumped semiconductor disk laser
Submitted for publication (2013).

Related publications not included in the thesis

The following journal papers and conference contributions by the author are related to the subject, but not included in the thesis.

- K. Seger, N. Meiser, S. Choi, B. H. Jung, F. Rotermund, O. Okhotnikov, V. Pasiskevicius and F. Laurell, *Carbon nanotube mode-locked semiconductor disk laser*, Optik och fotonikdagarna 2012, Oct. 18-19, Stockholm, Sweden.
- N. W. Meiser, K. Seger, V. Pasiskevicius, E. Rafailov, I. Krestnikov, *Quantum dot saturable absorber mode-locked Yb:KYW-laser with 1 GHz repetition rate*, Europhoton 2010, Aug. 29 - Sept. 3, Hamburg, Germany.
- K. Seger, B. Jacobsson, V. Pasiskevicius and F. Laurell, *Tuning and locking of a Yb:KYW laser with a transversally chirped volume Bragg grating*, EOS Topical meeting on Lasers 2009, Capri, Italy.
- K. Seger, P. Jelger, B. Jacobsson, V. Pasiskevicius and F. Laurell, *Using a Chirped Volume Bragg Grating to Tune a Passively Q-Switched Nd:YVO_4 Laser*, EOS Topical meeting on Lasers 2009, Capri, Italy.
- K. Seger, B. Jacobsson, V. Pasiskevicius and F. Laurell, *Use of a Transversely Chirped Volume Bragg Grating for Tuning a Yb:KYW Laser*, Northern Optics 2009, Vilnius, Lithuania.
- P. Jelger, K. Seger, V. Pasiskevicius, F. Laurell, *Spectral Narrowing of Highly Efficient Cryogenically Cooled Ytterbium Doped Fiber Lasers*, CThGG4, CLEO - Conference on Lasers and Electro-Optics, 1-5 June 2009, Baltimore, USA.
- K. Seger, P. Jelger, B. Jacobsson, V. Pasiskevicius, F. Laurell, *Tunable and Passively Q-Switched Nd:YVO_4 Laser Using a Chirped Volume Bragg Grating*, CTuB6, CLEO - Conference on Lasers and Electro-Optics, 1-5 June 2009, Baltimore, USa.
- K. Seger, B. Jacobsson, V. Pasiskevicius, F. Laurell, *Tunable Yb:KYW laser using a transversely chirped volume Bragg grating*, TuB15, aSSP - advanced Solid-State Photonics, February 1-4 2009, Denver, USA.
- J. Rautiainen, K. Seger, E. J. Saarinen, J. Lyytikäinen, V. Pasiskevicius, O. G. Okhotnikov, *Spectral control of frequency-doubled semiconductor disk laser using volume Bragg grating*, Europhoton 2008, Paris, France.
- K. Seger, J. Rautiainen, V. Pasiskevicius, O. G. Okhotnikov, *Narrowband intracavity frequency-doubled semiconductor disk laser with a volume Bragg grating*, LPHYS 2008, Trondheim, Norway.

Author contribution

My contributions in the original papers has been the following:

I I designed and performed the experiments together with Björn Jacobsson and wrote the paper with assistance from the co-authors.

II I designed and performed the experiments together with Niels Meiser and wrote the paper with assistance from the co-authors. The periodically-poled KTP crystal was provided by Carlota Canalias.

III I designed and performed the experiments together with Pär Jelger and assisted in writing the paper.

IV I performed the experiments together with Niels Meiser and assisted in writing the paper. The quantum-dot saturable absorber was supplied by Edik Rafailov and Igor Krestnikov.

V I performed part of the experiments together with Rene Hartke and assisted in writing the paper.

VI I designed and performed the experiments together with Niels Meiser and wrote the paper with assistance from the co-authors. Andrius Zukauskas and Carlota Canalias provided the periodically-poled Rb-doped KTP crystal.

VII I designed and performed the experiments together with Niels Meiser and wrote the paper with assistance from the co-authors. The gain structure was provided by Oleg Okhotnikov and the SWCNT saturable absorber was fabricated by Niels Meiser and Sun Young Choi and characterzied by Bo Hee Jung.

Preface

The research forming this thesis has been performed at the Laser Physics group at KTH, the Royal Institute of Technology, in Stockholm, from 2007 to 2013.

This work was supported by the Swedish Research Council (VR) through its Linnæus Center of Excellence ADOPT and the European Community FP7 FAST-DOT project under Grant agreement 224668.

Acknowledgements

This work was a long journey and it would not have been possible without the help and support from many people. I would like to thank:

Professor Fredrik Laurell, my main supervisor, for accepting me as a PhD-student in his group and giving me the chance to work on lots of different lasers. You always had time for discussions and helped me through the up and downs of a PhD-student's life.

Professor Valdas Pasiskevicius for guiding me through the world of an European Project, giving me valuable feedback on my work and sharing your vast experience in lasers and nonlinear optics.

Professor Fabian Rotermund and Sun Young Choi for helping kick-starting the carbon nanotubes activity in our group and giving valuable feedback for the absorber production and the experiments.

Professor Günter Huber for inspiring me with his laser physics lecture to start the diploma thesis in his group, which paved the way for this thesis. And of course the whole "Gruppe F" at the Institute of Laser Physics in Hamburg for welcoming me back for a few experiments and making my stays there fun.

Professor Oleg Okhotnikov and Jussi Rautiainen for giving me the chance to perform experiments at the ORC in Tampere, Finland and for helping me out with some gain chips.

Niels for sharing many hours in- and outside the lab, working on our lasers and discussing science and non-science.

All the people at the Laser Physics Group: Björn and Jonas for introducing me to the world of VBGs, Carlota and Andrius for fabricating and helping me with the PPKTP crystals, Pelle for giving me a shot at fiber lasers, Jens for his help with the courses and polishing my English, Martin for a lot of MAGIC lunches and, of course, all the others for having a great time at the conferences, coffee breaks and in the lab.

My family for backing me up during my life.

Very special thanks go to my wife Kirsten for her support during all these years. You followed me to Sweden and without you, this wouldn't have been possible. You make my life complete.

List of abbreviations and symbols

The following abbreviations and symbols are used in this thesis.

BPM	birefringent phase matching
CNT	carbon nanotube(s)
CVBG	(transversally) chirped VBG
cw	continuos wave
FWHM	full width at half maximum
IC	intra cavity
KTP	potassium titanyl phosphate
OPO	optical parametric oscillator
OPSDL	optically pumped semiconductor disk laser
PP	periodically poled
QPM	quasi-phase matching
SA	saturable absorber
SESAM	semiconductor saturable absorber mirror
SFG	sum frequency generation
SHG	second harmonic generation
SWCNT	single-walled carbon nanotube(s)
TPA	two-photon absorption
VBG	volume Bragg grating
ε_0	permittivity of free space
μ_0	permeability of free space
λ	vacuum wavelength
ν	frequency
$\omega = 2\pi\nu$	angular frequency
$\mathbf{k}$	wave vector
$k = \lvert\mathbf{k}\rvert = 2\pi n/\lambda = \omega n/c$	wave-vector magnitude
$c = 1/\sqrt{\mu_0\varepsilon_0} = \lambda\nu$	speed of light in vacuum
$v = \omega/k = c/n$	speed of light in a medium
$v_g = \partial\omega/\partial k = c/n_g$	group velocity
n	refractive index
n_2	nonlinear refractive index
n_g	group index
$\beta_2 = \partial^2 k/\partial\omega^2$	group-velocity dispersion
Λ	spatial period
$\chi^{(N)}_{jk\ldots}$	N^{th}-order electric susceptibility
$\tilde{\mathbf{E}}$	electric field
$\mathbf{E}$	complex amplitude of $\tilde{\mathbf{E}}$

Part I

Background and Overview

1

Introduction

The basics of the laser (**L**ight **A**mplification by **S**timulated **E**mission of **R**adiation) were laid by Albert Einstein with his work on emission and absorption of radiation [Ein16], [Ein17]. However, it took 40 years before Schawlow and Townes proposed a theoretical concept for a light source based on stimulated emission [Sch58]. Only two years later the first solid-state laser, a flash-lamp pumped ruby laser, was realized by Maiman [Mai60]. Yet another two years later, the first laser action in a semiconductor was demonstrated [Hal62], [Nat62], [Qui62].
Already in 1964, the first diode-pumped solid-state laser, an U^{3+}:CaF_2 crystal pumped by a GaAs laser diode, was demonstrated [Key64]. This was an important step for the construction of compact and efficient lasers, since diode-pumping enables precise tuning of the pump wavelength to the maximum absorption wavelength of the gain medium, which can give close to 100 % energy transfer to the ion. This is very efficient compared to flash lamp pumping, where only a minor part of the pump light is absorbed by the laser ion. The drawback of solid-state lasers is the limitation of the direct laser emission to the near infrared spectral range. However, this can be overcome by the use of second-harmonic generation, which was demonstrated as non phase-matched in quartz [Fra61] and later as birefringent phase-matched [Mak62], [Gio62]. With sum-frequency generation [Bas62] and difference frequency generation [DiD62] in non-linear crystals, the whole visible and ultraviolet spectral range becomes accessible. Those lasers are a very good alternative to the often inefficient and bulk liquid and gas lasers.
At first, the laser has been called "a solution looking for a problem" [Tow03]. This has changed drastically, as in today's daily life, lasers are used for many applications in medicine, material processing, telecommunication and for measurement techniques. The various applications have very different requirements for the laser: The most obvious is probably the wavelength, for example lasers used in display applications would need to be in the blue, green and red visible spectral range. A laser targeting the absorption of a specific atom or molecule would need to have exactly the corresponding absorption wavelength and at the same time, have a very stable

output in terms of wavelength. Another important parameter that determines the design of the laser is the needed average output power. The average power can range from typically one milliwatt for a semiconductor red laser pointer to many kilowatts for a CO_2 laser used in the industry for cutting.
A laser can also be designed for different modes of operation, which can be divided into continuous wave and pulsed operation. Continuous wave, or cw, lasers are emitting a stable output power over time with very little fluctuations in terms of power. Pulsed lasers on the other hand have a strong modulation of the output power over time. The emitted pulses can be in the range of nanoseconds for Q-switched lasers or in the range of femtoseconds for mode-locked lasers. The common trait is a peak power that is several orders of magnitude higher than the average output power of the laser. These pulsed lasers are very useful for applications that require a high peak-power such as nonlinear optics or material processing, or for applications that make use of the very short time scale for example for use in femto-chemistry.

In this work, I will show how volume Bragg gratings with a transversal chirp can be used for tuning of solid-state lasers. With this new method, intracavity elements are no longer needed for the wavelength tuning, as the volume Bragg grating replaces the output coupler. An experimental evaluation of the thermal limitations of volume Bragg gratings will be presented as well.
As mentioned above, mode-locked lasers are a very important laser source for a variety of applications. The commercial availablility of purified, single-walled carbon nanotubes has made it possible to produce saturable absorbers for mode-locking in an easy and cheap way. Here, I will present how such a saturable absorber with low losses can be used to mode-lock an optically-pumped semiconductor disk-laser, showing the versatility of both devices.
In addition to that, I will provide an experimental evalutation of the large amplitude fluctuations that can occur in intracavity frequency-doubled lasers. This will be performed for an optically-pumped semiconductor disk-laser, that typically has a very stable output. The special properties of a volume Bragg grating can reduce those fluctuations in a compact solid-state laser as well.

1.1 Outline

The next chapters describe the basic theory and concepts that are necessary for understanding the work in this thesis and will put the performed worked in an appropriate framework.

Chapter 2 covers the basic laser physics, and gives a short overview of the different types of solid-state lasers that were utilised throughout this work. In Chapter 3, volume Bragg gratings are described theoretically, followed by an overview of the different experiments utilising these gratings. After that, Chapter 4 covers the the-

oretical background of pulsed lasers and the experiments, where pulsed lasers have been constructed. Chapter 5 gives a short introduction to nonlinear optics with a focus on second-harmonic generation and a description of the actually demonstrated systems including second-harmonic generation. Finally the first part finishes in Chapter 6 with a conclusion and an outlook.
The second part consists of the papers that are the foundation of this thesis.

2

Solid-State Lasers

In this chapter, the basics of solid-state laser physics that are necessary in order to understand this work will be presented. It will start with the interaction of light and matter and a general description of a cw laser system using so-called rate equations. This will be followed by a more in-depth description of the laser systems that were used in this work.

2.1 Light and matter interaction

The mechanism of a laser is based on the interaction of light and matter. If electromagnetic radiation interacts with matter, the occuring processes can be divided into intra-ionic and inter-ionic processes. The focus here will be on the relevant intra-ionic processes. They can be either radiative or non-radiative; in the radiative processes photons are involved, in the non-radiative processes, phonons. Fig. 2.1 shows the three most important radiative processes. Let us consider any two energy levels E_0 und E_1, with the population numbers N_0 and N_1, and with $E_1 > E_0$, as shown in Fig. 2.1. If we now transfer this idea onto a solid-state system, we can assume that E_0, being the ground state of the system, is the energetically most favourable state, maximally populated in a thermal equilibrium. The state E_1 has a higher energy value, and therefore it is a so-called exited state. Between those two energy state, we have an energy difference of $E_1 - E_0$.

Absorption

We may talk about (stimulated) absorption, if the system in the ground state E_0 absorbs a photon of frequency ν with the value:

$$\nu = \frac{(E_1 - E_0)}{h}, \tag{2.1}$$

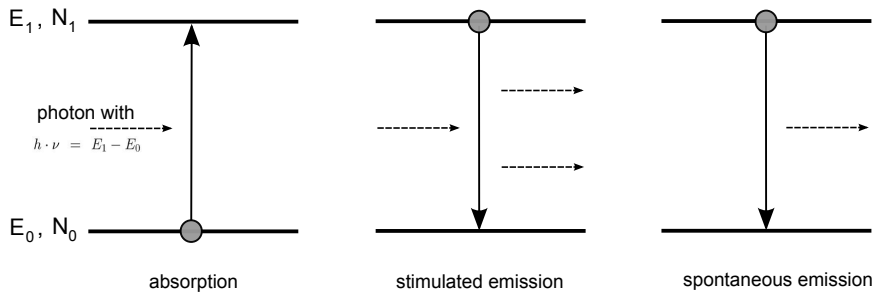

Figure 2.1: Intraionic processes.

in which the energy of the photon corresponds to the difference between the two involved energy levels, E_0 and E_1, with h being the Planck constant. The system is now in the exited state, E_1, after the absorption of the photon. The rate of the transition from E_0 to E_1, meaning the change with time of the population N_0 with time, must be proportional to the population of that state. So, we can write:

$$\left(\frac{dN_0}{dt}\right)_A = -W_{01}N_0. \tag{2.2}$$

The proportionality factor, W_{01}, describes the absorption rate and has the dimension of inverse time. For a plane wave, this factor depends on the cross-section, σ_{01}, of the transition $E_0 \rightarrow E_1$ and on the irradiating intensity, the photon flux F. With this, we can now write the equation as follows:

$$\left(\frac{dN_0}{dt}\right)_A = -\sigma_{01}FN_0. \tag{2.3}$$

Stimulated emission

If the system is in the exited state E_1, it can be stimulated by an incident photon of the same energy $E_1 - E_0$, to change it back to the ground state E_0. The transition $E_1 \rightarrow E_0$ can be described as the change of the population N_1 over time of the energy state E_1, which is proportional to the population of that state:

$$\left(\frac{dN_1}{dt}\right)_{St} = -W_{10}N_1. \tag{2.4}$$

The proportionality factor W_{01} corresponds to the emission rate and has also the dimension of inverse time. Just as in the case of absorption, it can be described

as the product of the cross section of the stimulated emission, σ_{10}, and the photon flux F. This results in the following relation:

$$\left(\frac{dN_1}{dt}\right)_{St} = -\sigma_{10} F N_1. \tag{2.5}$$

The photon that is generated by this process has the same direction, frequency, phase and the same polarisation as the incoming photon.

Spontaneous emission

By spontaneous emission we mean the transition of the system from the exited state E_1 into the ground state E_0 under the emission of a photon, the energy corresponds again to the difference between the two energy levels, E_1 and E_0. As the energy of the exited state E_1 is higher than the energy of the ground state E_0, the system tends to transit into the ground state spontaneously. The decay rate of the exited state E_1 has to be proportional to the population of the exited state E_1 and can be written as:

$$\left(\frac{dN_1}{dt}\right)_{Sp} = -A N_1. \tag{2.6}$$

The proportionality factor, A, is the so-called Einstein coefficient. It is inversely proportional to the spontaneous lifetime, τ_{Sp}, of the exited state E_1. With this, we can reformulate the equation 2.6 into:

$$\left(\frac{dN_1}{dt}\right)_{Sp} = -\frac{N_1}{\tau_{Sp}}. \tag{2.7}$$

2.2 CW lasers

A typical laser consists mainly of a few basic parts: An optical resonator, which consists of a highly reflective and a partially transmissive mirror; an active medium situated inside that resonator, and a pump source (see Fig. 2.2). The laser is based on the principle of the amplification of the photonnumber inside the resonator by stimulated emission. To accomlish this, it is necessary to achieve population inversion ($N_1 > N_0$) inside the gain medium. In an active medium with only two energy levels, population inversion is generally speaking not possible, because the population of the exited state can be only as high as the population of the ground state, which would mean that the emission is just as high as the absorption.

In a suitable system, with at least three involved energy levels, it is possible to create population inversion through the matching of the absorption of the active medium and the emission of the pump source, inside the active medium. If the amplification from the stimulated emission is higher that the resonator losses, the so-called threshold of the laser is reached and the laser starts to oscillate. A more in depth description can, for example, be found in the basic laser textbooks of Svelto [Sve89] and Siegman [Sie86].

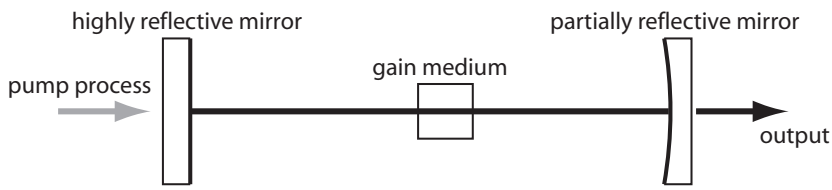

Figure 2.2: Schematic setup of a laser.

In order to describe the behaviour of a laser, so-called rate equations are commonly used. Here, we will concentrate on the rate equation of the cw case, a description of the rate equations of pulsed systems will follow in chapter four.
With the help of the population numbers of the involved levels N_i, the transition probabilities W_{ij}, and the number of photons q we can set up the rate equations. In this case we will concentrate on the rate equations of a classical 4-level-system and describe the derived results.

The 4-level-system

In the case of a 4-level-system, we assume that there is a fast phononic transition between the energy levels $E_3 \rightarrow E_2$ and $E_1 \rightarrow E_0$. With this, the fluorescence lifetime τ_1 and τ_3 of the energy levels E_1 and E_3 are much smaller than the fluorescence lifetime τ_2 of the energy level E_2 and with this argument we see that $N_3 \simeq N_1 \simeq 0$ and $N_2 > N_1$ under optical pumping.

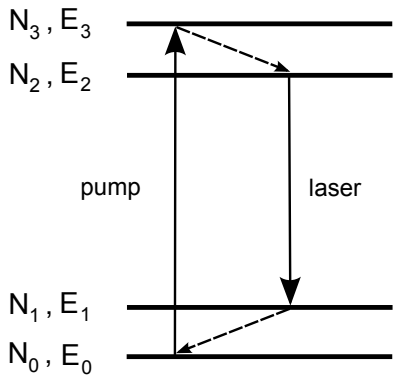

Figure 2.3: Schematic of a 4-level-system.

Using those boundary conditions, we get three rate equations, which describe the population N_i as well as the photon number q as a function of time [Sve89]:

$$\frac{dN_2}{dt} = W_p N_0 - \frac{N_2}{\tau} - BqN_2, \tag{2.8}$$

$$\frac{dq}{dt} = V_a BqN_2 - \frac{q}{\tau_c}, \tag{2.9}$$

$$N_t = N_0 + N_2. \tag{2.10}$$

Equation 2.8 describes the dynamic of the upper laser level N_2. It consists of the pump rate $W_p N_0$, the spontaneous emission rate $\frac{N_2}{\tau}$ and the stimulated emission rate BqN_2. The change of the number of photons inside the resonator is described by equation 2.9. It is composed of the growth rate of the number of photons by stimulated emission $V_a BqN_2$ and the decrease of the resonating photons through the losses inside the resonator $\frac{q}{\tau_c}$. Here, τ_c is the lifetime of the photons inside the resonator. It is assumed, that there is at least one photon present inside the resonator, to start the oscillation of the laser. The assumption $N_3 \simeq N_1 \simeq 0$ results in the total population N_t equation (2.10).

The parameter B introduced in the equations 2.8 and 2.9 describes the ratio of the emission cross section σ_{em} and the volume of the laser mode inside the active

medium V_a. As the index of refraction of the active medium with the length l is not equal to unity, we have to introduce an effective resonator length L' for the resonator with the physical length L, given by:

$$L' = L + (n_{eff} - 1)\, l. \tag{2.11}$$

Using this, we can now write B as follows:

$$B = \frac{\sigma_{em} \cdot l}{V_a} \cdot \frac{c_0}{L'}, \tag{2.12}$$

in which c_0 is the speed of light in vacuum.

Assuming $N \equiv N_2 - N_1 \simeq N_2$ inside the active medium, we can now convert the equations 2.8 and 2.9 together with equation 2.10 as follows:

$$\frac{dN}{dt} = W_p\,(N_t - N) - \frac{N}{\tau} - BqN, \tag{2.13}$$

$$\frac{dq}{dt} = V_a B N q - \frac{q}{\tau_c}. \tag{2.14}$$

Applied to the cw case, we get:

$$\frac{dN}{dt} = 0 \quad \text{and} \quad \frac{dq}{dt} = 0. \tag{2.15}$$

It follows for the threshold inversion N_{thr} from the equation 2.14 and with the use of equation 2.12:

$$N_{thr} = \frac{\gamma}{\sigma_{em} l} = \frac{1}{V_a B \tau_c}, \tag{2.16}$$

with the logarithmic total losses being defined as:

$$\gamma = \frac{L'}{\tau_c c_0}. \tag{2.17}$$

The threshold inversion is reached, when the amplification compensates the losses γ of one round trip. In this case, γ consists of the following parts:

$$\gamma = \gamma_i + \frac{\gamma_1 + \gamma_2}{2}, \tag{2.18}$$

$$\gamma_i = \text{logarithmic internal losses} = -\ln(1 - L_i), \tag{2.19}$$

$$\gamma_1 = \text{logarithmic losses at mirror 1} = -\ln(1 - T_1), \tag{2.20}$$

$$\gamma_2 = \text{logarithmic losses at mirror 2} = -\ln(1 - T_2). \tag{2.21}$$

The losses in this case originate from the losses at the mirrors (transmission T_i), as well as the losses inside the gain medium L_i.

In order to determine the necessary intensity of the pump radiation required to reach the threshold inversion, we can reformulate the equation for the threshold inversion (equation 2.17) and the inversion (equation 2.13) to get a condition for the threshold pump rate:

$$W_{thr} = \frac{N_{thr}}{(N_t - N_{thr})\,\tau} \approx \frac{N_{thr}}{N_t \tau} = \frac{\gamma}{N_t l \tau \sigma_{em}}. \tag{2.22}$$

At the threshold, and also below threshold, the number of the laser photons is nearly zero (see Fig. 2.4). Only when the pump rate W_p is larger than the threshold pump rate W_{thr}, the number of the laser photons will grow. It is convenient to write the photon number as follows:

$$q = V_a \tau_c \cdot \left[W_p \left(N_t - N_{thr} \right) - \frac{N_{thr}}{\tau} \right] = V_a N_{thr} \cdot \frac{\tau_c}{\tau} \cdot \left(\frac{W_p}{W_{thr} - 1} \right). \tag{2.23}$$

As we now have found an expression for q, we can now use equation 2.17 and equation 2.18 to calculate the output power P_i at the mirror i, which is proportional to the number of the laser photons:

$$P_i = \frac{\gamma_i c_0}{2L'} \cdot h\nu q. \tag{2.24}$$

Transient behaviour of a laser

A simulation of the rate equations will now be used to explain and to illustrate some important terms and the behaviour of the laser. In this case, rate equations in the form of

$$\frac{dN}{dt} = W_p - BqN - \frac{N}{\tau} \tag{2.25}$$

$$\frac{dq}{dt} = \left(V_a B N - \frac{1}{\tau_c} \right) q \tag{2.26}$$

were used. The simulation parameters can be found in table 2.2.

The simulation has been performed for two cases: For the behaviour of the population inversion and the laser photon number below the laser threshold and for the population inversion and the laser photon number above the laser threshold. The result can be seen in Fig. 2.4.

Parameter	Description	Value
B	Stimulated transistion rate per photon and Mode	$1 \cdot 10^{10}\ \frac{\mathrm{cm}^3}{\mathrm{s}}$
W_p	Pump rate	$6 \cdot 10^{14}\ \mathrm{s}^{-1}$
V_a	Mode volume	$1 \cdot 10^{-12}\ \mathrm{m}^3$
τ_c	Photon lifetime inside the resonator	$6 \cdot 10^{-8}\ \mathrm{s}$
τ	Fluoresence lifetime	$3 \cdot 10^{-6}\ \mathrm{s}$

Table 2.1: Simulation parameter for a 4-level-system.

Below the laser threshold, the population inversion grows until it reaches a maximum value for the specific pump rate, which again is limited by the number of available pump photons. The number of laser photons is close to zero in the beginning as the laser is not oscillating. An increase of the pump rate above the threshold pump rate leads to the start of the oscillation of the laser. This transient behaviour results from the interaction of the population inversion and the photon number. When the population inversion rises above the threshold inversion, the stimulated emission starts and the number of laser photons increases, because the laser photons will reduce the population inversion. This happens until the population inversion is below the threshold inversion. Then the photon number decreases and the population inversion increases, just so much that above the threshold inversion, the photon number can again decrease the population inversion. Therefore, the population inversion is oscillating around the threshold inversion. However, these oscillation amplitude become smaller, until they converge to the threshold inversion.

The laser photon number also converges to a fixed average value, which, in the begining, will show strong spikes because of the transformation of the population inversion. These spikes do become smaller with time until a constant number of photons is reached inside the resonator for the corresponding value. The number is proportional to the number of photons which are coupled out of the resonator and which in the end determines the output power of the laser.
The presented rate equation model is only valid for the case of one single longitudinal mode that is oscillating inside the resonator. If n modes are oscillating inside the resonator, this system has to be described by a set of $2n$ coupled first order differential equations. The equations must contain the amplitudes and phases of the modes, in order to take the interaction between the modes into account.

2.3 Bulk crystal lasers

The laser crystals desribed in this thesis are composed of a crystalline host material, which is doped with active laser ions. The ions employed belong to the rare-earth

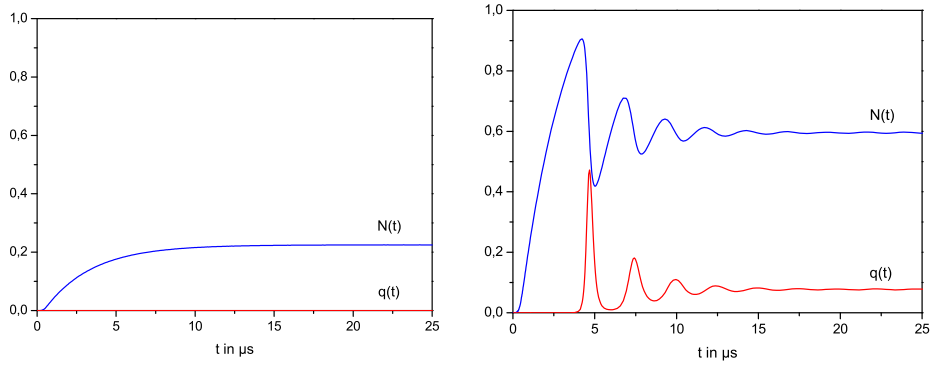

(a) Below threshold. (b) Above threshold.

Figure 2.4: Simulation of the inversion $N(t)$ and the photon number $q(t)$ for a 4-level-system.

elements or lanthanides, which is the group of elements with atomic numbers 57 to 71. They are characterised by a partially filled $4f$ electron shell in contrast to the fully filled $5s$-, $5p$- and $6s$-orbitals. When they are inserted into the host crystal, they pass three electrons on to the crystal lattice. Dipole-transitions in the $4f$ electron shell are now weakly allowed because of the influence of the crystal host field on the trivalent ion. They feature, in comparison to the allowed dipole transitions, a low energy and a long lifetime, making them ideal as laser ions. A detailed description of the theory of rare earth metals can be found in the book by Henderson and Imbusch [Hen89] and additionally in Powell [Pow98].
As the electrons in the $4f$-shell are screened against the crystal field by the $5s$- and the $5p$-shells, which are further away from the core, the energy states of the laser ions behave as a first approximation as the states of a free ion. The crystal field is then taken into account as a perturbation.

In order to calculate the electron states and their energies, the appropriate Hamilton operator has to be formulated and the associated Schrödinger equation has to be solved. However, the lanthanides represent a multi-particle system which does not have an exact analytical solution. To simplify the system, it is assumed that each electron is in an effective, spherically symmetric, central potential, which is formed by the attraction of the atomic core and the averaged repulsion of the other electrons. A direct interaction between the electrons is neglected [Lin96],[Mes90]. Using thses arguments, the Hamiltonian H_0 of an N-electron system can be written as follows:

$$H_0 = \sum_{i=1}^{N} \left(-\frac{\hbar^2}{2m_e} \Delta_{r_i} + V(r_i) \right), \tag{2.27}$$

with $-(\hbar^2 \Delta_{r_i}/2m_e)$ as the kinetic and $V(r_i)$ as the potential energy of the i-th electron in a distance r_i from the atomic core in the effective central field. The resulting energy eigenvalue equation is given by:

$$H_0 \Psi_0 = E_0 \Psi_0, \tag{2.28}$$

which, in our case, is separable and, taking into account the Pauli principle, results in the solution:

$$\Psi_0 = \prod_{i=1}^{N} |n_i l_i m_l m_s\rangle . \tag{2.29}$$

The wave function Ψ_0 is taken as the Slater-determinant [Sla29] from the spin- and stationary wave functions for the solution of the one-dimensional problem. The energy eigenvalues of these eigenstates are only dependent on the main quantum number n_i and the angular momentum quantum number l_i. The magnetic quantum number m_l and the spin quantum number m_s are degenerated.

With help of the Hartree-Fock method [Sza89], it is iteratively possible to determine a self-consistent central potential. This is done by starting from an arbitrary potential $V(\mathbf{r}_i)$ and use the calculated function from the Hartree-Fock equations as the new starting point, which will converge against the self-consistent potential $V(r)$.

In these calculations, the repulsion between the electrons and the spin-orbit interaction is neglected and has to be included as correction terms, H_C and H_{LS} shown below:

$$H_C = \sum_{i<j=1}^{N} \frac{e^2}{4\pi\epsilon_0 r_{ij}} - \sum_{i=1}^{N} \left(-\frac{Ze^2}{4\pi\epsilon_0 r_i} + V(\mathbf{r}_i) \right), \tag{2.30}$$

$$H_{LS} = -\sum_{i=1}^{N} \frac{1}{2m^2 c_0^2} \frac{1}{r_i} \frac{dV(\mathbf{r}_i)}{dr_i} (\mathbf{s}_i \cdot \mathbf{l}_i) . \tag{2.31}$$

The Hamiltonian for a free electron can now be written as:

$$H = H_0 + H_C + H_{LS}. \tag{2.32}$$

The added corrections result in a splitting of the $4f$-state into ${}^{2S+1}L_j$ states, and with J as the total angular momentum of the electrons. The result is different, depending on which correction term H_C or H_{LS} is most strongly affecting the energy levels:

I For the case that the influence of H_{LS} is smaller than the influence of H_C, it is called Russel-Saunders- or LS-coupling. Here, the total angular momentum $\mathbf{J}$ is the sum of the angular momentum $\mathbf{L}$ and the spin $\mathbf{S}$:

$$\mathbf{J} \quad = \quad \mathbf{L} + \mathbf{S}. \tag{2.33}$$

Here, $\mathbf{L} = \sum_{i=1}^{N} \mathbf{l}_i$ and $\mathbf{S} = \sum_{i=1}^{N} \mathbf{s}_i$ are given by the coupling of the angular momentum and the spin. The LS-coupling describes lighter elements very well.

II For heavier elements, H_C has a higher influence than H_{LS}. The spin and the angular momentum of each electron are now coupled directly into the resulting angular momentum $\mathbf{j}_i = \mathbf{l}_i + \mathbf{s}_i$ and the total angular momentum is given as:

$$\mathbf{J} = \sum_{i=1}^{N} \mathbf{j}_i. \tag{2.34}$$

This coupling is known as jj-coupling.

The influence of the correction terms for the lanthanides is similar, so an intermediate coupling has to be used. Linear combinations of LS-states with the same total angular momentum J result in states, which are named after the LS-state with the highest part in the linear combination. This gives rise to the possibility of an overlap between the different ${}^{2S+1}L$ multiplets with respect to their J-components, in which the total angular momentum J stays as a quantum number. The quantum numbers L, S, J and M are now the eigenvalues and the ${}^{2S+1}L_J$ states are $(2J+1)$-times degenerated in respect to M_j [Hen89]. The other perturbation terms like spin-spin and orbit-orbit or hyperfine interaction are negligible.

On contrast to this, the interaction of the crystal field is very important for the lanthanides, the splitting of the ${}^{2S+1}L_J$ is of the order of 10^3 cm^{-1}.

Influence from the crystal field

The $(2J+1)$-times degeneration of the ${}^{2S+1}L_J$ states are canceled because of the interaction of the lanthanide's $4f$-electrons with the electro-static field of the ligands

in the crystal. In order to describe that interaction, the Hamiltonian has to be suplemented by the following term:

$$H_S = -e\sum_{i=1}^{N}\mathbf{E}(\mathbf{r}_i)\cdot\mathbf{r}_i. \tag{2.35}$$

The degeneration of the former M_j energy levels, as a result of the crystal field, is a result of the Stark-effect and therefore known as the Stark-splitting and is usually of the order of around 100 cm$^-$1 and with that, one order of magnitude smaller than that of the other perturbation terms (see fig 2.5). With the help of the Kramers-theorem, this results in a splitting of maximum $(2J + 1)$ levels for the possible states for the ions with an even number of electrons. Ions with an uneven number of electrons, like neodym will split into $(2J + 1)/2$ Stark-levels. This splitting is a result of time-reversal invariance [Mes90]. If we take all of the interactions into account, the Hamiltonian now takes the following form:

$$H = H_0 + H_C + H_{LS} + H_S. \tag{2.36}$$

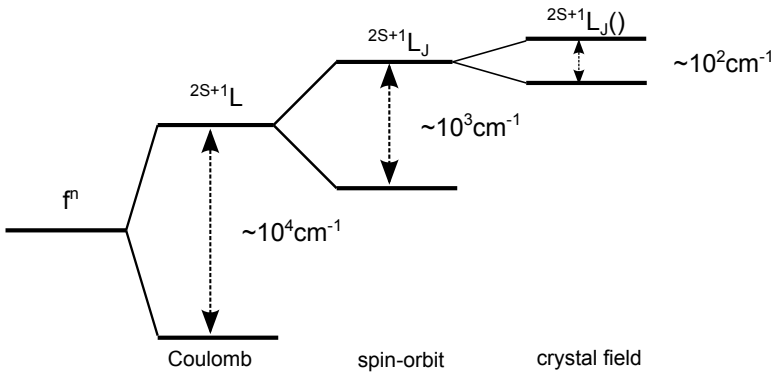

Figure 2.5: Schematic picture of the various influences of the pertubation terms on the energy levels of a rare-earth ion.

The following subsections present an overview of the laser crystals described in this thesis. A more in-depth overview of solid-state lasers and different laser crystals has been written by Huber et al. [Hub10].

Nd:YAG

The crystal $Y_3Al_5O_{12}$ (YAG) is probably the most popular and well-known host material for laser ions. It is an optically isotropic crystal and can be produced in

a very high optical quality using the Czochralski method. It has a high thermal conductivity of 13 $Wm^{-1}K^{-1}$. The Nd-doping in this material is typically of the order of one atomic percent, where the Nd-ion takes the place of an yttrium ion in the host lattice. The lifetime is 250 μs for the $^4F_{3/2} \rightarrow {}^4I_{11/2}$ transition, which corresponds to an emission wavelength of 1064 nm with a bandwidth of 0.8 nm and an emission cross section of $29{\cdot}10^{-20}$ cm^2. The laser crystal is typically pumped with diode lasers at 808 nm and has an absorption cross section of $7.9{\cdot}10^{-20}$ cm^2 [Cze02].

Nd:YVO_4

YVO_4 is a tetragonal, optically uniaxial crystal. It has two long a-axis and one short c-axes. For incident light whose electric field is polarized parallel to the c-axis (π polarization), the emission and absorption cross sections are much stronger than for a polarization parallel to an a-axis (σ polarization). The thermal conductivity is, with a value of 5.1 $Wm^{-1}K^{-1}$, less than one half of that of YAG's. However, the high emission cross-section and polarization-dependent emission makes YVO_4 a suitable candidate for many applications. The Nd-doping is also typically of the order of one atomic percent, where the Nd-ion takes the place of an yttrium ion in the host lattice as well. The lifetime is 97 μs for the transition $^4F_{3/2} \rightarrow {}^4I_{11/2}$ which corresponds to an emission wavelength of 1064 nm. The emission bandwidth is 1 nm with an emission cross section of $123{\cdot}10^{-20}$ cm^2 for the π polarization and a bandwidth of 1.5 nm and an emission cross section of $52{\cdot}10^{-20}$ cm^2 for the σ polarization. The laser crystal is typically pumped with diode lasers at 808 nm and has an absorption cross section of $60{\cdot}10^{-20}$ cm^2 for the π and $12{\cdot}10^{-20}$ cm^2 for the σ polarization, respectively [Cze02].

Yb:KYW

The double-tungstate host material $KY(WO_4)_2$ (KYW) is a biaxial crystal that has good mechanical properties with a thermal conductivity of 3 $Wm^{-1}K^{-1}$. The polarization axis n_m has the highest cross sections and was used in the experiments described in this thesis. The only involved energy levels for the laser transition are $^2F_{5/2} \rightarrow {}^2F_{7/2}$. But since lasing is possible from three different Stark sub levels in combination with vibronic broadening [Hel07], Yb:KYW has a broad emission between 995 nm and 1063 nm. The lifetime of the upper laser level is 232 μs with an emission cross section of $3{\cdot}10^{-20}$ cm^2. The system is typically pumped at 981 nm with an absorption cross section of $18.8{\cdot}10^{-20}$ cm^2. As the pump wavelength is close to the laser wavelength, the Yb:KYW laser features a low quantum defect, allowing it to build very efficient lasers. Yb:KYW is, in contrast to the Nd-doped crystals at 1064 nm, a three-level system, resulting in a higher threshold for lasing.

2.4 Semiconductor disk lasers

The general concept of optically pumped semiconductor disk lasers (OPSDL)[1] is similar to the well-known thin disk lasers [Gie94]. The major advantage of this concept is a high output power while maintaining a good beam quality. The concept was transfered to a semiconductor media, in which a semiconductor quantum-well structure is used as the gain material [Kuz97]. This laser combines the attractive features of potential for power scaling, excellent beam quality and wavelength flexibility. The active medium of a OPSDL is a semiconductor chip, which consists of a DBR-mirror[2], an active multi quantum well structure and a window layer (see fig. 2.6). The highly reflective DBR-mirror serves as one of the cavity mirrors and consists of alternating AlAs/GaAs layers in the near infrared spectral range.

The reflectivity of such a DBR-mirror is given by [She95]:

$$R = \left[\frac{n_0(n_2)^{2N} - n_2(n_1)^{2N}}{n_0(n_2)^{2N} + n_2(n_1)^{2N}}\right]^2 . \tag{2.37}$$

In this case, n_0 is the refractive index of the surrounding medium, n_1 and n_2 are the index of refraction of the alternating materials, and n_s is the index of refraction of the substrate. N is the number of alternating pairs. Very high reflectivity can be obtained this way. As an example, for a DBR-mirror at the wavelength of 1050 nm on a GaAs substrate with $n_{\mathrm{GaAs}} = 3.4826$, $n_{\mathrm{AlAs}} = 2.9543$ and $N = 30$ respectively, a reflectivity of $R = 0.99928$ is achieved. The bandwidth $\triangle\nu_0$ of the so-called stop-band around the central frequency ν_0 is given by:

$$\triangle\nu_0 = \frac{4\nu_0}{\pi} \arcsin\left(\frac{n_2 - n_1}{n_2 + n_1}\right). \tag{2.38}$$

In the case mentioned above, this would correspond to a bandwidth of 175 nm. By increasing the number of alternating pairs and the difference of the index of refraction, the reflectivity as well as the bandwidth will increase.

The active multi-quantum well structure is located directly next to the DBR-mirrors. It consists of a periodic arrangement of InGaAs-quantum wells, for emission in the near-infrared, which are positioned exactly on $\frac{\lambda}{2}$-intervals of the desired wavelength λ between the GaAs-barriers. This ensures that the maximum of the standing wave inside the cavity will be at an optimum position.

The pump radiation will primarily be absorbed in the barriers and thereby producing free carriers, which then relax into the InGaAs quantum wells, where they

[1] Also known as vertical, external-cavity surface-emitting lasers (VECSEL)
[2] DBR = *distributed Bragg reflector*

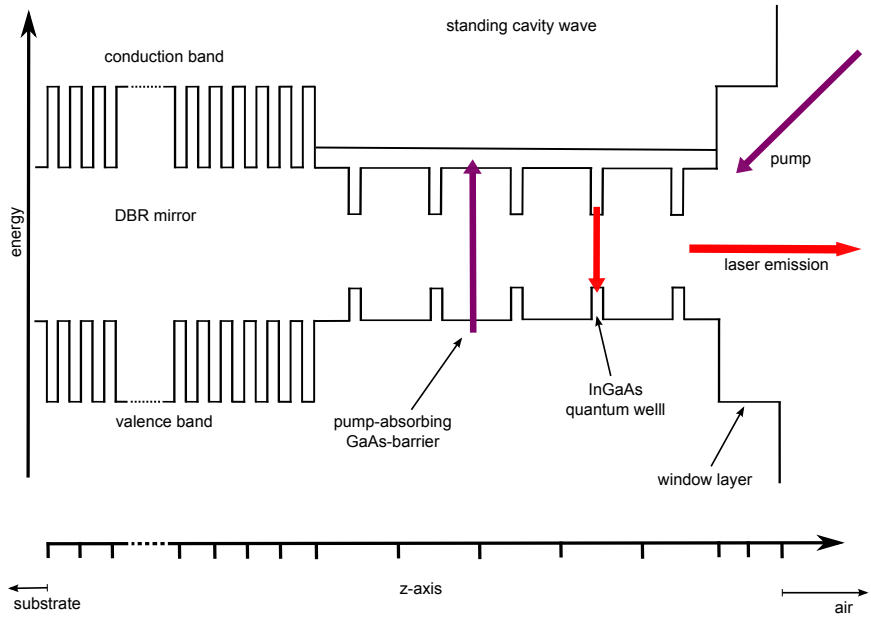

Figure 2.6: Band diagram of a semiconductor disk laser.

create population inversion. Here, they recombine under stimulated emission.

In order to prevent the charge carriers from diffusing into the chip surface, an AlAs window layer with a large bandgap serves as a barrier to the surface, which will prevent the diffusion.

The description of the recombination as mentioned above involves an optical transition via the electron distribution in the conduction- and the valence-bands. If the semiconductor is in thermal equilibrium, it is explained through the Fermi-Dirac statistics. The probability $f(E)$ that an electron is in a state of the energy E at a given temperature T is given by the expression [Tro06]:

$$f(E) = \frac{1}{1+\exp\left[(E-E_F)/k_BT\right]}, \tag{2.39}$$

where k_B is the Boltzmann constant and E_F is the Fermi-energy. To find an expression for the Fermi-Dirac statistics in the case of optical pumping, the description of the different energy levels involved is needed. In Fig. 2.7 an optical transition with photon energy E between the conduction band of energy E_c and the valence band energy E_v respectively, is shown.

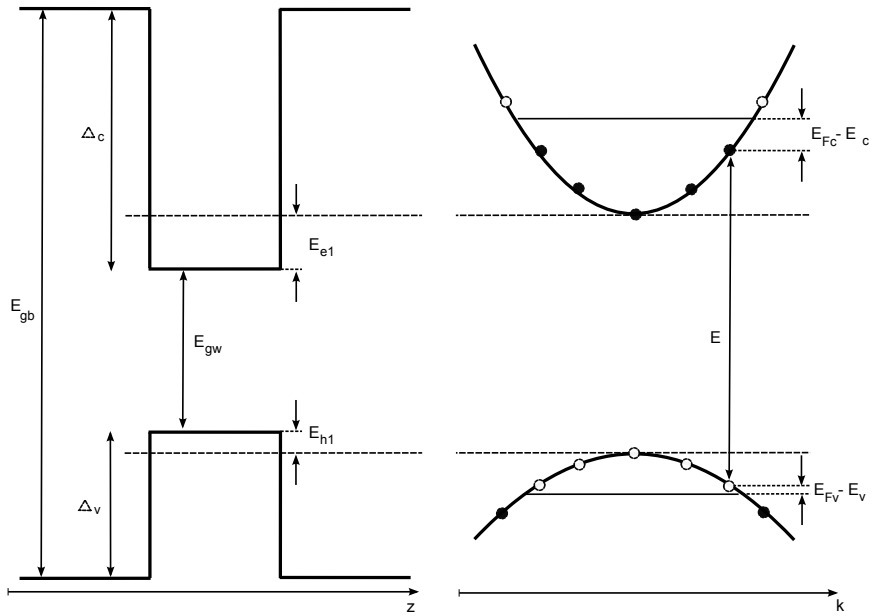

Figure 2.7: Energy levels of a quantum well [Tro06].

Using a parabolic approximation for the bands (the effective mass is considered to be energy and temperature dependent), the energy of the emitted photon can be expressed as follows:

$$E = E_{gw} + E_{e1} + E_{h1} + \frac{\hbar^2 k^2}{2m_e} + \frac{\hbar^2 k^2}{2m_h} \tag{2.40}$$

In this expression E_{gw} is the band gap energy of the quantum well, E_{e1} and E_{h1} are the confinement-energies of the first bound state in the conduction and valence band, E_{bd} is the bandgap of the barrier layer and m_e and m_h are the effective masses of the electron and the hole respectively. The states have the same direct wavenumber k for an optical transition. The Fermi-Dirac distributions for both states are given by:

$$f_c = \frac{1}{1 + \exp\left[(E_c - E_{Fc})/k_B T\right]} \quad , \tag{2.41}$$

$$f_v = \frac{1}{1 + \exp\left[(E_v - E_{Fv})/k_B T\right]}. \tag{2.42}$$

If we assume a parabolic approximation for the first bound states in the quantum well, the Fermi energies in the valence and the conduction band can be put in a

direct relation with the electron- and hole concentrations and with that, the number of charge carriers per area of the quantum well can be calculated. In total, charge neutrality is assumed, which means that $N_e = N_h = N$. The Fermi energy for the two bands can now be expressed as:

$$E_{Fc,v} = k_B T \ln\left[\exp\left(\frac{N_{e,h}\pi\hbar^2}{m_{e,h}k_B T}\right) - 1\right] \tag{2.43}$$

This expression is valid for the population density of one quantum well. In general however, the population of all of the quantum wells is different. But, if the active medium is constructed in a way that all quantum wells have the same charge carrier density, the transversal charge carrier profile in all quantum wells will be similar. With this supposition, one can write down the amplification, or gain, per unit time:

$$\langle G \rangle = \frac{\Gamma_t \Gamma_z G_0}{V}(f_c - f_v). \tag{2.44}$$

Here, V describes the mode volume in air for a cavity of the length L, see fig. 2.8. The output mirror M, has a radius of curvature R, which together with the well-known g-parameter $g = 1 - \frac{L}{R}$, makes us write the following expression for the mode volume:

$$V = \frac{1}{2}\lambda L^2 \sqrt{\frac{g}{1-g}}. \tag{2.45}$$

The parameter G_0 is an intrinsic property of the quantum well, Γ_t is the transversal and Γ_z the longitudinal confinement-factors. A more in-depth description can be found in, for example, [Tro04] and [Tro06].

OPSDL laser setup

A schematic setup of an OPSDL can be seen in fig. 2.8. It consists of a DBR-miror together with the active medium (called chip in the following) as one unit. This chip structure is bonded onto a heat sink. The laser cavity is then formed by the chip and an output coupling mirror M. The whole system is optically pumped under an angle.
In order to improve the heat managment of the chip under strong optical pumping, a diamond heat spreader can be bonded onto the chip, in order to dissipate the heat more effectively.

The transient behaviour of the laser can be modelled using rate-equations as desribed earlier this chapter. However, here they describe the temporal development

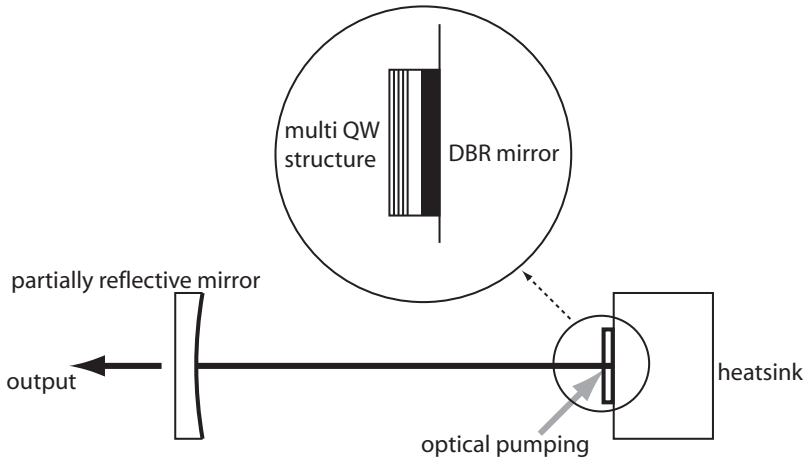

Figure 2.8: Schematic setup of an OPSDL.

of the charge carriers N in a quantum well in a region of Q quantum wells, the charge carriers N_R of all of the barriers together and the number of photons ϕ in the resonator [Tro06]:

$$\frac{dN}{dt} = \frac{(\eta_c N_R - N)}{\tau_R} - \frac{N}{\tau(N)} - G(N)\phi, \tag{2.46}$$

$$\frac{\partial N_R}{\partial t} = \Pi - Q\frac{\eta_c N_R - N}{\tau_R} - \frac{N_R}{\tau_c}, \tag{2.47}$$

$$\frac{d\phi}{dt} = G(N)\phi + \Gamma_t \Gamma_z \beta_{sp} B N^2 - \frac{\phi}{\tau_\phi}. \tag{2.48}$$

It is assumed that each quantum well possesses the charge carrier population $\eta_c N_R$ under optical pumping. The population relaxes with the lifetime τ_R, given by the charge carrier dynamics. The η_c is defined by the height of the confinement potentials. The lifetime of the charge carriers in the quantum wells $\tau(N)$ can be approximated by the following expression:

$$\frac{N}{\tau(N)} = AN + BN^2 + CN^3. \tag{2.49}$$

The three terms describe the defect recombination A, spontaneous, radiative recombination B and Auger rekombination C. The rate the charge carrier reservoir in the barriers is pumped with, is given by the intensity of the incident pump light I_p, which pass over into the active region. Together with the in the active region absorbed pump rate η_p at a pump wavelength λ_p this results in:

$$\Pi = \eta_p \frac{I_p}{\frac{hc}{\lambda_p}}. \tag{2.50}$$

The spontaneous recombination BN^2 is weighted by the longitudinal and transversal confinement factor. The factor of the spontaneous emission β_{sp} is defined by the part of the spontaneous emitted power, which is associated with the fundamental mode of the external cavity. The photon lifetime τ_ϕ is determined by the resonator round-trip time and can be treated as equivalent with it.

In this simple model, the temperature dependancies of the band gap and that of the index of refraction are not taken into account. In addition, quasi particle effects are neglected. Despite this, the effective gain and the photon dynamics for a OPSDL can be properly described. Temperature-dependent phenomena such as thermal rollover and the redshift that occurs with increasing temperature, however, can not be described by this model.

2.5 Fiber lasers

An optical fiber usually consists of two parts, the core and the cladding. The light is confined inside the fiber core through total internal reflection from the cladding, which has a lower index of refraction. The difference in the index of refraction defines the cone under which light can be coupled into the fiber core and is called the numerical aperture (NA) of the fiber with the acceptance angle θ_a:

$$NA = \sqrt{n_2^2 - n_1^2} = \sin(\theta_a) \tag{2.51}$$

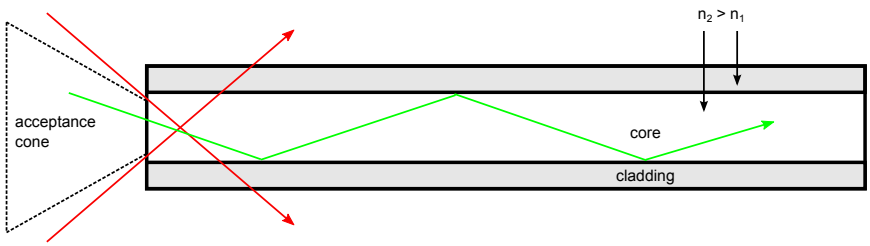

Figure 2.9: Schematic setup of a fiber.

The core of a fiber with optical gain consists usually of lanthanide ions doped into a silica glass, while the cladding is undoped SiO_2 with a lower index of refraction (see fig. 2.9). The diameter of the core is between 8 μm and 30 μm, while

the diameter of the cladding is more than one order of magnitude larger, normally around 125 μm or larger.

The advantage of fiber lasers in comparison with bulk crystal lasers is directly dedused from their peculiar form. Since the gain medium is very thin and long, the surface to volume ratio becomes large, which facilitates efficient heat removal and a very efficient cooling of the fiber is possible. This allows the construction of high power lasers in the range of several kW of continous-wave output power. The second benefit of having an elongated gain medium, where the light is guided, is the good beam quality even at very high output powers without any heat distortion. Due to the length of the gain medium, very high pump absorption can be achieved with low doping concentrations and with that, very efficient lasers with high gain can be constructed. Typically the polished or cleaved end-surface of the fiber has enough reflection to serve as the output coupling mirror. A more detailed description can be found in [Jel09].

3

Volume Bragg Gratings

This chapter describes the theoretical background of volume Bragg gratings, followed by an overview of the experiments, that used said gratings as cavity mirrors.

3.1 Overview

Volume Bragg gratings (VBGs) are basically a piece of photo-thermo-refractive (PTR) glass with a refractive-index modulation written into the material [Efi99]. This is done by light exposure in the ultra-violet spectral region, followed by a heat treatment. The main advantage of VBGs is that the reflection properties can be engineered and reflections as high as 99.7 %, with a bandwidth as low as a few hundred pico-meters can be fabricated. This allows the use of VBGs as highly reflective mirrors in laser cavities. With this, it is possible to lock the operational wavelength of a laser to exactly the desired value. This is not possible with using dielectric mirrors, where additional intracavity elements are needed to stabilise the spectrum.
With VBGs, several lasers and optical parametric oscillators (OPO) have already been realised from our group who pioneered this field. I would like to mention the following results:

OPO A VBG-locked optical parametric oscillator [Jac05], a narrow linewidth, 2 μm OPO in periodically poled $LiNbO_3$ with volume Bragg grating output coupler [Hen07] and an investigation of the spectrum of multi-longitudinal mode pumped near-degenerate OPOs with volume Bragg grating output couplers [Hen09].

Single-mode laser A tunable, single-longitudinal-mode ErYb:glass laser [Jac06], and a single-longitudinal mode laser in Nd with a Bragg-grating Fabry-Perot cavity [Jac07a].

Yb-lasers A quasi-two-level Yb:KYW laser [Hel07] and a widely tunable Yb:KYW laser with a volume Bragg grating in a retro-reflector setup [Jac07b].

Fiber lasers An efficient, narrow-linewidth VBG-locked Nd:fiber laser [Jel07a], a tunable narrow-linewidth Yb-doped fiber laser [Jel07b], a narrow linewidth high output coupling dual VBG-lcoked Yb-doped fiber-laser [Kim08] and a narrow linewidth high output coupling dual VBG-locked Yb-doped fiber-laser [Jel10].

For all these publications, commercially available VBGs written in PTR glass were used. In table 3.1, a list of some important VBG material parameters is presented:

Parameter	Description	Value
n_0	refractive index	1.49 [Gle92], [Efi99]
α	thermal expansion coefficient	8.4 ppm/K [Zwa06]
dn/dT	thermo-optic coefficient	0.05 ppm/K [Ven05]
n_2	nonlinear refractive index	$3.3 \cdot 10^{-20}$ m^2/W [San06]
d_{th}	damage threshold	10 J/cm^2 [Efi99b], [Gle04]

Table 3.1: Volume Bragg grating material parameters.

3.2 Theoretical description

In the following part, the important steps for the derivation of the reflectivity R_{max} and the bandwidth $\Delta\lambda$ of a given VBG with a grating period Λ of a thickness d will be presented.The grating properties were already described by Kogelnik in 1969 using a plane-wave approximation. This means that the electric field of the incident wave M and the reflected wave N are only dependent of the propagation direction z. The Bragg condition can now be described in terms of the wave-vectors $\mathbf{k_{N,M}}$[1]:

$$\mathbf{k}_N = \mathbf{k}_M - \mathbf{K} + 2\delta. \tag{3.1}$$

The grating is defined by the grating vector $\mathbf{K}$ and by δ, the wave-vector mismatch, which allows non-perfect phase matching in order to obtain the bandwidth of the grating. If we assume that the wavelength is the same for the incident and for the reflected light, the wave-vectors can be written as $k_{N,M} = 2\pi n_0/\lambda \equiv \beta$. The grating vector can now be expressed in terms of the grating period Λ, so that $|\mathbf{K}| = 2\pi\Lambda$. For perfect phase matching, the wave-vector mismatch δ is zero and we

[1] Vectors and tensors will be written in bold letters.

obtain the well known formulation of the Bragg condition from equation 3.1 with λ_B as the so-called Bragg wavelength:

$$-\beta \cdot \mathbf{e}_z = \beta \cdot \mathbf{e}_z - K \cdot \mathbf{e}_z \Rightarrow \lambda_B = 2n_0\Lambda. \tag{3.2}$$

The Bragg wavelength is the wavelength for which the grating will have the highest reflection. We assume that the grating modulation can be written as $n(z) = n_0 + n_1 \cdot f(z)$. In this equation n_0 is the average refractive index and n_1 the modulation strength of the grating. For a sinusoidal variation of the index of refraction, $f(z)$ can be expressed as a Fourier expansion with only two non-zero coefficients (only first order diffraction):

$$f(z) = \sin(Kz) = \frac{1}{2i}\left(e^{iKz} - e^{-iKz}\right). \tag{3.3}$$

In order to fully describe the grating, the peak reflectivity as well as the bandwidth of the grating have to be determined. For this we need to describe the wave inside the grating and if we assume that the incident light is polarised along the y-axis, the planar wave can be written as:

$$\left(\nabla^2 + \beta^2 + 4\beta\kappa f(z)\right) E(z) = 0. \tag{3.4}$$

As discussed earlier, the electric field is a superposition of the incident field M and the reflected field N and takes the form of:

$$E(z) = M(z) + N(z) = \widetilde{M}(z) \cdot e^{-ik_M z} + \widetilde{N}(z) \cdot e^{ik_N z} \tag{3.5}$$

$$\tag{3.6}$$

inside the grating. If the light is incident from the negative z-axis, the boundary conditions are:

$$\widetilde{M}(0) = M_0 \tag{3.7}$$

$$\widetilde{N}(d) = 0 \tag{3.8}$$

With these boundary conditions, and employing the slowly-varying-envelope-approximation as well as letting all fast oscillating terms average to zero, we can formulate the coupled-wave equations as follows:

$$\frac{d\overline{M}}{dz} = i\delta\overline{M} + \kappa\overline{N}, \tag{3.9}$$

$$\frac{d\overline{N}}{dz} = \delta\overline{M} - i\kappa\overline{N}. \tag{3.10}$$

In this formulation of the coupled wave equations, the field amplitudes were transformed to $\widetilde{M} = \overline{M} \cdot e^{-i\delta z}$ and $\widetilde{N} = \overline{N} \cdot e^{i\delta z}$ respectively. The solution is obtained by the eigenvalues $\gamma = \pm\sqrt{\kappa^2 - \delta^2}$ and the eigenvectors $(\pm\gamma + i\delta, \kappa)$, which result in the following equations with

$$M(\delta, z) = M_0 t(\delta, z) e^{-i(k_M+\delta)z}, \tag{3.11}$$
$$N(\delta, z) = M_0 r(\delta, z) e^{i(k_N+\delta)z}, \tag{3.12}$$

as the electric field inside the grating. The transmission and the reflection coefficients $t(\delta, z)$ and $r(\delta, z)$ are given by:

$$t(\delta, z) = \frac{-\gamma \cosh\left(\gamma(d-z)\right) + i\delta \sinh\left(\gamma(d-z)\right)}{-\gamma \cosh(\gamma d) + i\delta \sinh(\gamma d)}, \tag{3.13}$$
$$r(\delta, z) = \frac{\kappa \sinh\left(\gamma(d-z)\right)}{-\gamma \cosh(\gamma d) + i\delta \sinh(\gamma d)}, \tag{3.14}$$

respectively. Those expressions can be used to calculate the total power reflectivity:

$$R(\delta) = \left|\frac{N(\delta, 0)}{M(\delta, 0)}\right|^2 = |r(\delta, 0)|^2 = \frac{\kappa^2 \sinh^2\left(\sqrt{\kappa^2 - \delta^2} \cdot d\right)}{\kappa^2 \cosh^2\left(\sqrt{\kappa^2 - \delta^2} \cdot d\right) - \delta^2}. \tag{3.15}$$

The maximum reflectivity R_{max} is obtained for $\delta = 0$:

$$R_{max} = \tanh^2(\kappa d), \tag{3.16}$$

with κ as the coupling strength. The last important parameter to calculate is the bandwidth of the grating. Here it is defined as the spectral distance between the two closest zeroes around the peak. They are positioned at $\delta = \pm\sqrt{\kappa^2 + \pi^2/d^2}$ and with that the total spectral bandwidth can be found to be given by:

$$\Delta\lambda_B = \lambda_B \sqrt{\left(\frac{n_1}{n_0}\right)^2 + \left(\frac{2\Lambda}{d}\right)^2} \tag{3.17}$$

For strong gratings, the FWHM bandwidth $\Delta\lambda_{FWHM}$ is equal to $\Delta\lambda_B$, however for weak gratings with a lower peak reflectivity, $\Delta\lambda_{FWHM} = 0.44 \cdot \Delta\lambda_B$. Now we can describe the VBG by either its optical properties, the peak wavelength λ_B, peak reflectivity R_{max} and the bandwidth $\Delta\lambda$ or by its material properties, such as the grating period Λ, refractive index modulation n_1 and the thickness d. Fig. 3.1 shows the simulation and measurement of a VBG used in this work.
A more detailed description for the plane wave theory can be find in [Hel08], which includes a description for finite beams.

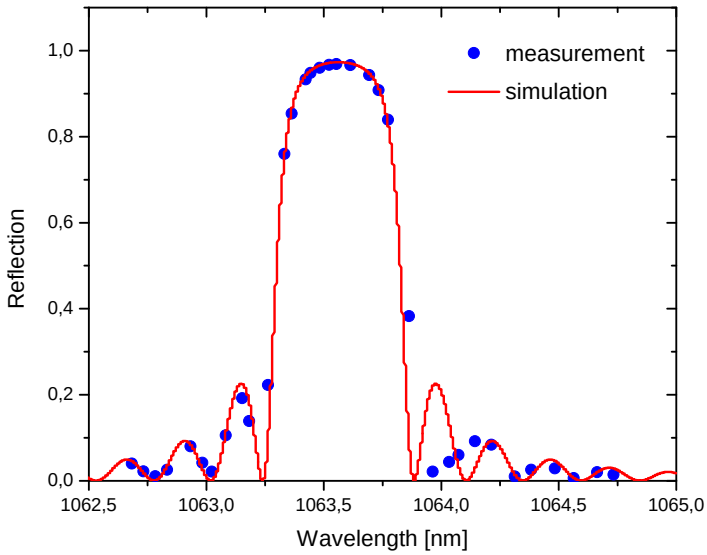

Figure 3.1: Measuremt and simulation for a VBG.

3.3 Narrow bandwidth operation experiments

It is challenging to construct single-frequency lasers in relatively long cavities, since the number of modes that can oscillate in the cavity grows rapidly, as they have to fulfill the boundary conditions of a standing wave. With this, the possible oscillating modes inside the resonator are defined by:

$$\nu_m \quad = \quad m \cdot \frac{c_0}{2nL} \quad \text{mit} \quad m = 1, 2, 3, ... \tag{3.18}$$

However, only modes that are in the amplification range of the active medium can oscillate. This is called the gain profile of the active medium. It is in general much broader than the possible cavity modes. Because of this, there are several resonator modes inside the gain profile, which can oscillate, if no further mode-selecting elements are present inside the laser resonator.

Below some of the lasers, and laser experiments this thesis is built on, are described.

OPSDL with stable, narrow bandwidth operation

The emission wavelength of an OPSDL is temperature dependent, thus it is worth to evaluate the use of a VBG to fix the operating wavelength and reduce the spectral bandwidth of the laser. In the laser cavity, the VBG replaces an ordinary dielectric output coupler and therefore no additional intra-cavity elements are needed, thus making the setup simple and stable. For the evaluation, it is necessary to compare the performance of the laser when using a VBG with an ordinary output coupler regarding output power, spectrum and wavelength stability.

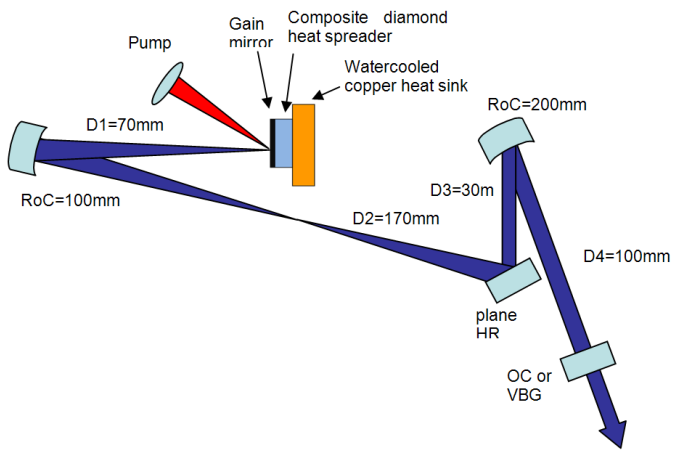

Figure 3.2: Schematic setup of the laser cavity.

To investigate the use of a VBG, a z-type cavity (see Fig. 3.2) was constructed. The cavity consisted of the gain structure in the first beam waist and the cavity was completed by the VBG as an output coupler. For comparison, the VBG could be replaced by an ordinary plane dielectric mirror. In addition, two highly reflective curved dielectric mirrors were utilized to control the cavity mode waist.
The semiconductor gain structure was grown by molecular beam epitaxy for an emission wavelength of 1055 nm. The structure includes a highly reflective Bragg mirror formed by 29-pairs of AlAs/GaAs layers and the gain region was composed of 7 GaInAs quantum wells engineered for the stated emission wavelength. The structure was grown on n-type GaAs, which was etched away after the growth to improve the heat dissipation.

In the laser setup, the semiconductor chip was mounted on a water-cooled copper heatsink at 15 °C with a 300 μm thick composite diamond heatspreader between the semiconductor structure and the heatsink to enhance the thermal control. The gain structure was optically pumped by a fibre-coupled 808 nm laser diode at an angle of 35 degree, focused to a spot size of 180 μm ($1/e^2$ radius). The VBG reflection peak was centered at 1055 nm with a measured reflectivity of 99.8% (disregarding loss) and with a spectral bandwidth of 0.4 nm (FWHM). The VBG (Optigrate Inc.) was antireflection coated for 1055 nm.

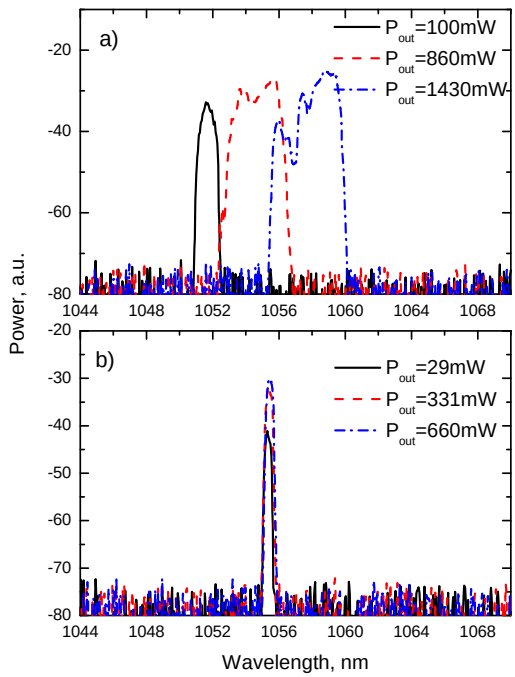

Figure 3.3: Spectrum for the fundamental radiation using a) a HR dielectric mirror or b) a VBG as output coupler.

We investigated the laser operating at the fundamental wavelength and the behavior using the VBG or an ordinary dielectric output coupler with 99 % reflectivity were both studied. In the case of the ordinary output coupler with a reflectivity

of 99 %, the laser spectrum shifted to longer a wavelength and broadened with increasing pump power (see Fig. 3.3). From the threshold and up to a maximum output power of 1.47 W at a pump power of 15 W, the laser wavelength shifted from 1052 nm to 1058 nm and the bandwidth increaseed from 1 nm to 4 nm. When the normal output coupler was replaced by a VBG, the spectrum remained stable at the grating wavelength of 1055 nm and was narrowed to a spectral bandwidth of 0.5 nm for all output powers (see Fig. 3.3). All the spectral measurements were performed with an optical spectrum analyzer with a resolution of 0.05 nm.

The output power for the two systems is shown in Fig. 3.4. As can be seen, the threshold is quite similar for both cases, but for the VBG, thermal rollover occured already at a pump power of 8 W, instead of at 15 W for the normal output coupler. The studied gain structure had a positive detuning so that its subcavity resonance wavelength at room temperature was 1050 nm and the quantum well emission at 1031 nm. The gain spectrum red shifted three times faster than the subcavity thickness with increasing pump power. At high pump power the subcavity resonance was at longer wavelength than the fixed operation wavelength leading to lowered gain. As the VBG locked the operating wavelength, the laser was not able to follow the shift to longer wavelength with increasing pump power, which resulted in a stronger sensitivity to the heat load and therefore in an earlier thermal roll over. It should be noted that the rather modest laser power for the fundamental was the result of a too low output coupling of the VBG for good IR extraction.

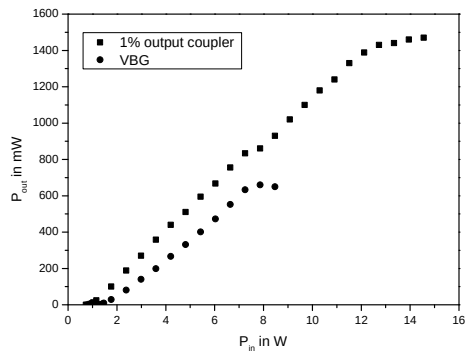

Figure 3.4: Laser output powers with the dielectric mirror and the VBG as output coupler.

An Yb:KYW laser with a VBG incoupling mirror

As VBGs can have a very narrow reflection spectrum and are essentially transparent to other wavelengths than the Bragg wavelength, they can be also used as the input coupler in a diode-pumped solid-state laser arrangement without disturbing the pump laser [Hel07], [Hag07]. This leaves considerable freedom in designing the rest of the cavity for generation of high beam quality and for example efficient frequency doubling. In a V-shaped cavity for example, two curved dielectric mirrors can be used to create two small beam waists in the nonlinear crystal and the laser crystal respectively, while the VBG locks the wavelength at the designed wavelength, eliminating any need for additional IC elements such as etalons.
However, the VBG can limit the performance of the laser, since the absorption in the grating, though small, will lead to a decrease of its reflectivity. In order to investigate these possibilities, we decided to build such a laser and explore these properties.

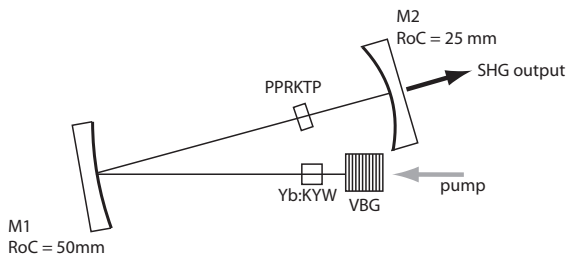

Figure 3.5: Setup for the laser cavity, including a PPRKTP crystal that could be inserted for SHG.

The used laser features a simple V-type cavity design, with the VBG serving as input coupler, see Fig. 3.5. Two highly reflective curved dielectric mirrors were utilized to control the cavity mode waist. The cavity was completed by the VBG as the input coupler. The VBG (Optigrate Inc.) had a size of 5x5x3 mm^3, a peak reflectivity of 99.5 % at a center wavelength of 1029 nm with a bandwidth of approximately 0.3 nm.

A transfer matrix model was used to calculate the VBG's diffraction efficiency and the laser intensity inside the VBG. The un-chirped grating had a sinusoidal refractive index modulation with an amplitude of $3.8{\cdot}10^{-4}$ around an average refractive index of 1.49 and a Bragg wavelength of 1029.5 nm. The model alters the grating period and the refractive index according to the temperature distribu-

tion in the VBG using the thermal expansion coefficient α = 8.5 x 10^{-6} K^{-1} and $dn/dT = 0.5 \cdot 10^{-6} K^{-1}$.
A 3D finite element model (FEM; COMSOL Multiphysics 4.3) was used to calculate the temperature distribution with regard to the absorbed power distribution. The absorbed power was described by a scaling parameter $\alpha_{abs} I_{circ}$ and a distribution function. Here, α_{abs} is the absorption coefficient and I_{circ} is the intra-cavity intensity. In the transverse direction the distribution function was modeled as a Gaussian beam with constant beam radius (ω = 45 μm), and in the propagation direction of the beam the distribution function was provided by the grating model described above. The simulation finds converged solutions for incremental steps of the scaling parameter, $\alpha_{abs} I_{circ}$.

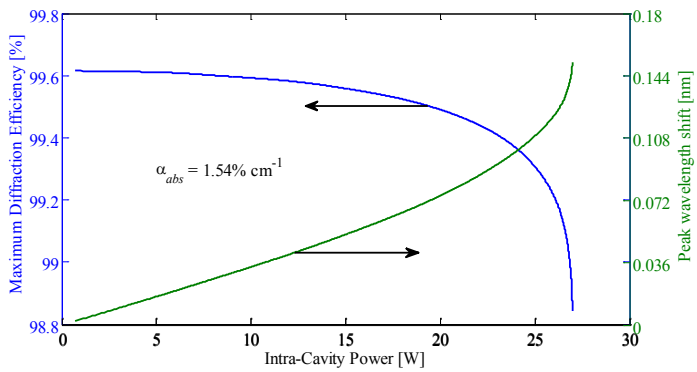

Figure 3.6: Simulation for the VBG employed in our experiment showing the change of reflectivity and the corresponding center wavelength with increasing intracavity power.

The results show that an intra-cavity power limit of 27 W corresponds to an absorption coefficient of 1.54%cm^{-1}. As seen in Fig. 3.6, the maximum diffraction efficiency remained high for intra-cavity powers up to approximately 26 W, where it rapidly decreased. It should be mentioned that the absorption for this VBG is unusually large, and a roll-off of the type seen here should normally be expected at considerably higher powers. Pumping through the VBG provides a simple cavity design with a good control of the beam size in the laser and PPRKTP crystals, and it has negligible effect on the VBG spectrum as the pump wavelength is non-resonant.
The absorption will limit the available intracavity power and with that the conversion efficiency of the SH. The compact folded setup provided efficient and stable

SHG at 515.5 nm, with an output power of 1.1 W, using PPRKTP at 80 °C, more information on the frequency doubling will be given in chapter V.

This experiment is described in more detail in paper VI.

A Cryogenically cooled fiber laser

Cryogenic cooling can improve the performance of crystalline laser materials, as the low temperature reduces the thermal expansion and the thermooptic coefficient as well as increases the thermal conductivity. In addition, the thermal populatuion of the lower laser levels is reduced in Yb-doped lasers and, as a consequence, the reabsorption losses are minimized for fiber lasers and self-pulsing is suppressed or elliminated. This leads to a more efficient laser operation at the cost of a broadened linewidth. However, the broadened linewidth can easily be reduced by using a VBG as a cavity mirror .

To explore these features, a fiber laser was constructed, using double-clad Yb-doped large-mode-area fibers. The fibers had a core diameter of 20 μm and a cladding diameter of 400 μm with corresponding NA of 0.06 and 0.22, respectively. On all fibers, one of the fiber ends was perpendicularly cleaved to provide 4 % cavity feedback while the other was angle-polished to prevent parasitic reflections.

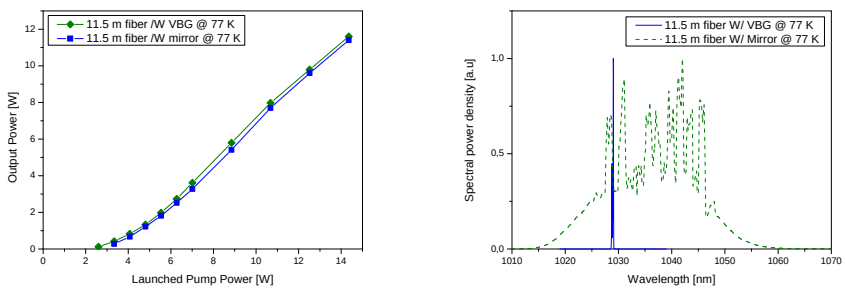

Figure 3.7: Comparison of outout power and spectrum for a cryogenic cooled fiber with dielectric output coupler and VBG.

A VBG or a highly-reflective (HR) mirror was placed on the angle polished side of the fiber. The VBG had a bandwidth of 0.4 nm and a diffraction efficiency of 99.9 % at the center wavelength of 1029.5 nm. The surface of the VBG was AR-coated to prevent parasitic reflections. The fiber was coiled and placed in a Styrofoam liquid nitrogen container.
Fig. 3.7 shows the experimental data for the 11.5 m long fiber at liquid nitro-

gen temperature (LNT). The emission linewidth in case of the HR mirror is almost 20 nm. When the mirror was exchanged for the VBG, the output power did not change noticeably, but the spectral characteristics changed considerably as the linewidth now was reduced to 0.4 nm. The temporal characteristics showed very little fluctuations, less than a few per cent regardless of launched pump power. The broadening of the emission linewidths at LNT with the mirror is attributed to a flattening of the inversion threshold for wavelengths above 1 μm in combination with a decreasing homogeneous broadening.
In conclusion, we demonstrated the use of a VBG for spectral narrowing of a Cryogenically cooled fiber laser with no loss in power compared to the same laser with broad emission spectrum due to the use of a dielectric mirror instead of the the VBG.

This experiment is described in more detail in paper III.

3.4 Tuning with chirped VBGs

Tunable lasers have numerous applications in areas such as spectroscopy and material characterization. The laser performance of tunable lasers is governed by two main factors, the available gain bandwidth in the laser material and the utilized spectral filtering to enable tunable operation.
The filter that performs the spectral discrimination in a tunable laser should optimally provide the following properties:

I The spectral selectivity should be sharp with a wide free spectral range, so that the laser can operate with as a narrow bandwidth as possible, and should not jump to neighboring orders of the filter.

II The method for tuning the filter should be simple, preferably by adjusting just one degree of freedom.

III The filter should not introduce additional losses, that will reduce the efficiency.

IV Insertion of the filter should not complicate the laser cavity setup, to keep it compact and stable.

The most common methods are an intracavity prisms [Li06], surface gratings [Moe66] and birefringent filters [Pet07] and etalons [Col63]. However, they do not fulfill all of the above mentioned properties.
Tuning with VBGs can be achieved either by turning the VBG to change the Bragg condition as for example in a retro reflector setup [Jac07b] or in the fabrication process by changing the Bragg condition over the length of the glass, i.e. a chirped grating. This new method fulfills all of the above mentioned properties and is presented in two different experiments in the papers I and II.

Wavelength tuning of an Yb:KYW laser using a chriped volume Bragg grating output coupler

A transversely chirped volume Bragg grating (CVBG) can be used as a very simple way to obtain tunable solid-state lasers. In particular, we have investigated the Yb:KYW laser crystal, but other laser ions and host materials could also be used. Currently, the grating fabrication technology limits the reflectivity of the transversely chirped gratings to about 60 % [2], meaning that high-gain laser materials should be used. Furthermore, our work demonstrates that CVBGs can be used in a very alignment sensitive system such as a 3-level solid-state laser, which demonstrates the good uniformity of the component.

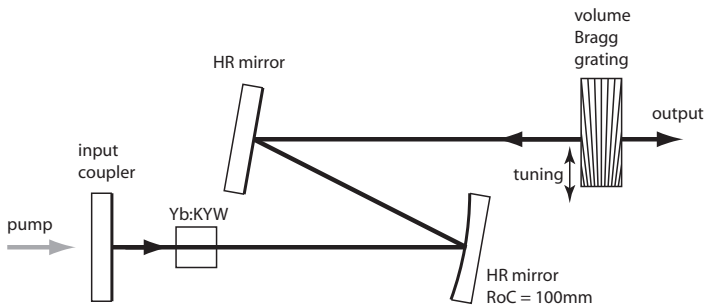

Figure 3.8: Setup of the laser cavity.

The constructed laser cavity was simple and compact, depicted in Fig. 3.8. The z-shaped cavity consisted of an input coupler, the laser crystal, two folding mirrors and finally the transversally chirped volume Bragg grating as output coupler and spectral selector. The chirped volume Bragg grating was used simultaneously as tuning element and output coupler of the laser cavity. The grating was AR coated and had an aperture of 5 mm x 20 mm. The maximum grating reflectivity was around 50 % going from 996 nm to 1017 nm, with a chirp rate of 1.1 nm/mm. The grating bandwidth at a single point was 0.37 nm FWHM. The grating was mounted on a translation stage for easy tuning by displacement of the grating orthogonal to the laser direction.

For the measurement of the tuning range, the grating was realigned at every measurement point in order to obtain maximum output power. However, tuning over the whole range without realignment was also possible, only resulting in a moderate power reduction of about 25 %. By measuring how much realignment was needed due to the grating, we could conclude that the chirped grating was

[2]Personal communication with *Optigrate Inc.*

slightly curved by 1 ± 0.3 mrad over the tuning range. It should be pointed out that the angle between the grating planes due to the chirp is only 0.4 μrad, and has no practical impact on the laser alignment. The linearity of the grating chirp was also investigated, by comparing the grating position to the laser wavelength. The deviation from a linear behaviour between 998 nm and 1015 nm was ± 0.01 %, relative to the grating period, with an overall parabolic-like shape.

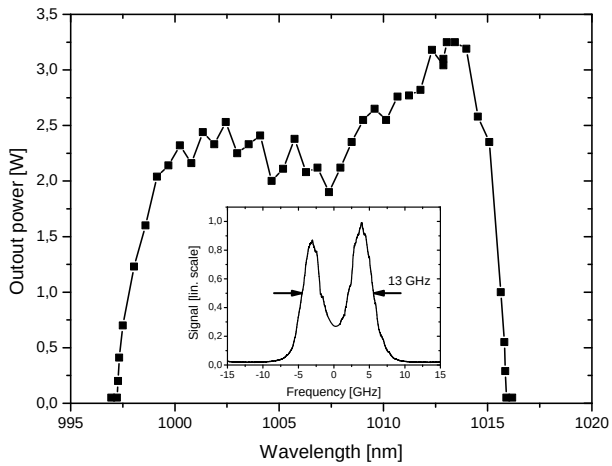

Figure 3.9: Laser tuning range at maximum pump power. Inset shows the laser spectrum measured with a scanning Fabry-Pérot interferometer.

In our diode-pumped Yb:KYW laser, the wavelength could be continuously tuned from 997 nm to 1016 nm by simply translating the transversely chirped volume Bragg grating. The maximum laser power was 3.3 W, with a spectral bandwidth of 13 GHz (see Fig. 3.9).

This experiment is described in more detail in paper I.

Single-longitudinal mode operation and tuning of a Nd:YVO_4 laser using a chriped volume Bragg grating output coupler

A CVBG was also used to tune a diode pumped Nd:YVO_4 laser in a simple, linear and compact plane-plane cavity using only two, or three, elements to form the laser, see Fig. 3.10. The chirped VBG (CVBG) had a tuning range from 1054 nm to 1065 nm with a chirp-rate of 0.81nm/mm. The reflectivity was reduced from approximately 75 % at the shortest wavelength to 20 % at the longest wavelength.

With a beam size of 100 μm in the cavity the linewidth was below 0.1 nm.

A Cr^{4+}:YAG saturable absorber was used to obtain passive Q-switching. Up to 4 W of output power was obtained with a tuning range of 2 nm for continuous wave (cw) operation and 1.08 W of average power in the Q-switched regime with a pulse length of 3.9 ns and with a repetition rate of 150 kHz at 1064.1 nm. When Q-switched, the laser oscillated on a single longitudinal mode (SLM).

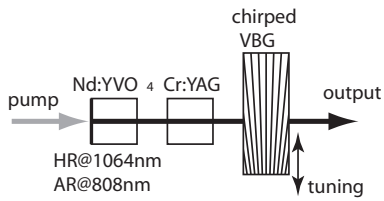

Figure 3.10: Setup of the laser cavity.

It was not obvious, that the laser was oscillating on a SLM, as the longitudinal mode separation of the cold cavity was roughly 50 pm, so more than one longitudinal mode should be able to oscillate, as the bandwidth of the CVBG was 0.4 nm. To further investigate this, the transmission of the CVBG was simulated at the center wavelength λ=1064.2 nm together with the transmission of the Fabry-Perot formed by the Nd:YVO_4 laser crystal (3 mm) and with the air gap between the Nd:YVO_4 laser crystal and the Cr^{4+}:YAG saturable absorber (0.1 mm). From this we found that every second longitudinal mode suffered losses from the Fabry-Perot formed by the end surfaces of the laser crystal. Longitudinal modes, which are even more separated from the main peak, suffered additional losses from the increasing transmission of the CVBG and from the Fabry-Perot, which is resulted from the small air-gap between the laser crystal and saturable absorber. This resulted in the laser oscillating only at a single longitudinal mode, even at higher output powers (see Fig 3.11).
The transient behaviour of this laser will be described in chapter 4.

This experiment is described in more detail in paper II.

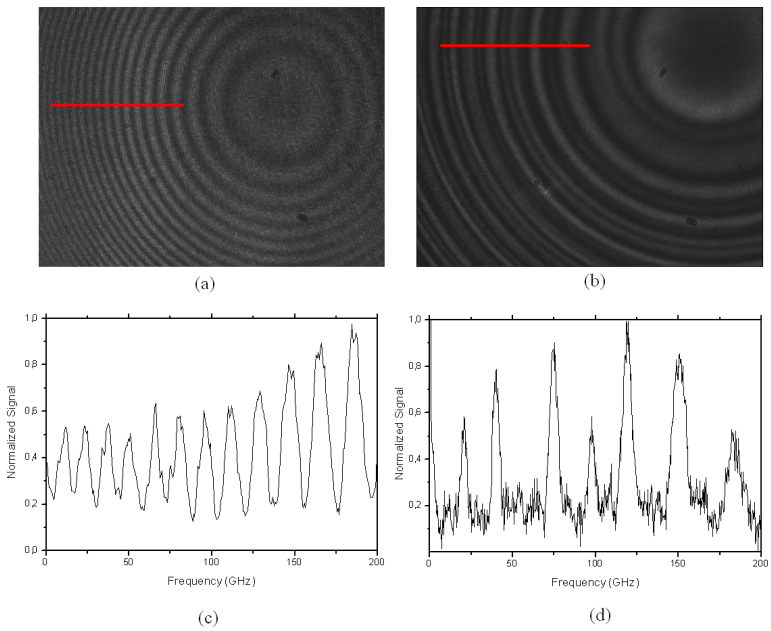

Figure 3.11: The longitudinal mode spectrum as determined using a Fizeau interferometer with a free spectral range of 21 GHz . The symmetric pattern in a) shows that the laser is operating single-mode. The picture b) shows the multi-mode pattern obtained when the laser was operating using a dielectric output coupler with the same reflectivity. The graphs c) and d) show a cross-section (marked with a red line) of the intensity distribution in a) and b) to visualize single-mode and multi-mode operation, respectively.

4

Short Pulse Generation

This chapter desribes transient behaviour of lasers, starting with Q-switching theory followed by experiments connected to Q-switching. The second part contains the basics of passive mode-locking with the related experiments.

4.1 Overview

For many laser applications, high powers are often wanted or needed. A prominent example is material processing, where lasers are used to cut, solder and to mark a variety of materials. Another application is nonlinear frequency conversion, since the conversion efficiency scales with the intensity of the fundamental wave. A pulsed laser provides output peak power often orders of magnitude higher than the average power of the same laser. Pulsed solid-state lasers are normally either Q-switched of mode-locked. For Q-switching, it can be as simple as putting a Cr:YAG crystal in a laser cavity, but especially the extreme cases of mode-locked few-cycle attosecond pulses and high average power Q-switched lasers, are challenging from both the scientific and the engineering perspective.

4.2 Q-switching

Q-switched lasers have been investigated for a long time[Mcc62] and are still attracting attention due to their wide range of applications in industrial and research areas. Of particular interest are high pulse energies facilitating material processing as well as high peak power, enabling efficient non-linear optics. When compared to mode-locked systems, Q-switched systems are more tolerant with respect to the laser design parameters, a fact that simplifies their construction and operation. Furthermore, when using passive saturable absorbers additional electronics can be avoided. The most commonly used saturable absorbers for Nd-based lasers are Cr:YAG crystals [Shi95], [Das96]. Recently Q-switching using single-walled carbon

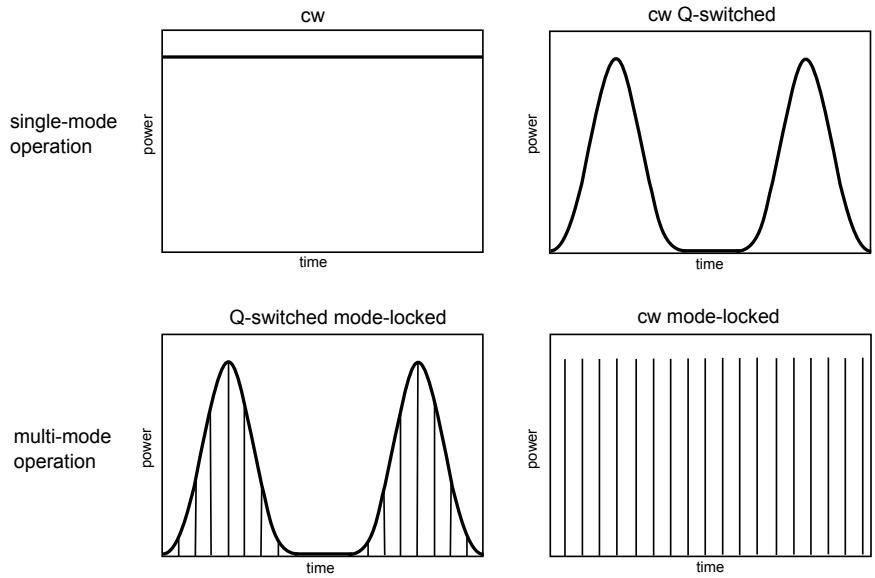

Figure 4.1: Different modi operandi for a laser.

nano tubes has been presented in a Nd:LuYGdVO$_4$ laser [Che11] and in a Nd:YAG ceramic laser [Li12].

The term Q-switching originates from the so-called Q-factor (quality factor), which is defined as the ratio of the stored energy to the loss per cycle. If a laser is Q-switched, the quality (losses) of the laser is switched periodically. For continuous pumping, when the losses are high, lasing is suppressed and energy is stored in the gain medium. When the losses are switched off, the laser is suddenly above threshold and the stored energy is released into a short pulse. The switching can be achieved by active means with, for example, acousto-optic or electro-optic modulators or by using passive Q-switches such as Cr:YAG saturable absorber crystals (SA).

Passive Q-switching

Passive Q-switches allow a simple and compact laser design, since the only required element is a SA without any external driver. In the case of a Cr:YAG crystal, it can be as small as a few mm^3 and may be easily inserted into the laser cavity. The performance ranges from ps pulses in micrco cavities to high power ns pulses in large lasers.

Passive Q-switching can be described using the following set of three coupled

parameter	description
γ_g	decay rate of upper laser level
γ_a	decay rate of first excited state of Cr^{4+}
γ	population reduction factor, equals 1 for an ideal four-level laser
K_g	coupling constant $K_g = \frac{2\sigma_g}{t_r A_g}$, with the cross section σ_g of the induced laser emission, the cavity round-trip time t_r and the effective beam cross-section A_g
K_a	coupling constant $K_g = \frac{2\sigma_1}{t_r A_a}$, with the cross section σ_1 of the absorber ground level and the effective beam cross-section within the absorber A_a
N_{a0}	N_a just before the switching process

Table 4.1: Parameters for the passive Q-switching rate equations of a 4-level laser with Cr^{4+}.

rate-equations, taking into account the population in the saturable absorber as well as the exited-state absorption [Sie86]:

$$\frac{dn(t)}{dt} = [K_g N_g(t) - K_a N_a(t) - \beta K_a \left(N_{a0} N_a(t)\right) - \gamma_c] \cdot n(t), \tag{4.1}$$

$$\frac{dN_g(t)}{dt} = r - \gamma_g N_g(t) - \gamma K_g N_g(t) n(t), \tag{4.2}$$

$$\frac{dN_a(t)}{dt} = \gamma_a \left(N_{a0} - N_a(t)\right) - K_a N_a(t) n(t). \tag{4.3}$$

Where the key variables are explained in table 4.2.

This set of coupled nonlinear differential equations does not have an analytical solution, but can be solved numerically. This has been done by X. Zhang et al [Zha97] and they derived the following set of analytical equations for calculating the pulse energy E_P, the peak power P_{peak}, the pulse length τ_P, the pulse repetition rate f_P and the average output power P_{avg} as follows:

$$E_P = \frac{h\nu A_a}{2\sigma_g \gamma} \ln\left(\frac{1}{R}\right) \cdot \ln\left(\frac{n_i}{n_f}\right), \tag{4.4}$$

$$\begin{aligned} P_{peak} = {} & \frac{h\nu}{\gamma t_r} \ln\left(\frac{1}{R}\right) \\ & \cdot \left[n_i - n_t - n_{t0} \ln\left(\frac{n_i}{n_f}\right) - (n_i - n_{t0}) \frac{1}{\alpha} \left(1 - \frac{n_t^\alpha}{n_i^\alpha}\right)\right], \end{aligned} \tag{4.5}$$

$$\tau_P \approx \frac{E_P}{P_{peak}}, \tag{4.6}$$

$$f_P = \frac{1}{\tau_a} \frac{\frac{P}{P_{thr}} - \left(1 + \frac{1}{\beta}\right)/2}{1 - \frac{1}{\beta}}, \tag{4.7}$$

$$P_{avg} = f_P \cdot E_P, \tag{4.8}$$

with:

$$n_i = \frac{\ln\left(\frac{1}{R}\right) + \ln\left(\frac{1}{T_0^2}\right) + L}{2\sigma_g A_a^{-1}}, \tag{4.9}$$

$$n_{t0} = \frac{\ln\left(\frac{1}{R}\right) + \frac{1}{\beta}\ln\left(\frac{1}{T_0^2}\right) + L}{2\sigma_g A_a^{-1}}, \tag{4.10}$$

$$\frac{n_t}{n_i} = \frac{n_{t0}}{n_i} + \left(1 - \frac{n_{t0}}{n_i}\right)\left(\frac{n_t}{n_i}\right)^{\alpha}, \tag{4.11}$$

$$\frac{n_f}{n_i} = 1 + \left(\frac{n_{t0}}{n_i}\right)\ln\left(\frac{n_f}{n_i}\right) - \left(1 - \frac{n_{t0}}{n_i}\right)\frac{1}{\alpha}\left[1 - \left(\frac{n_f}{n_i}\right)^{\alpha}\right], \tag{4.12}$$

$$\alpha = \frac{\sigma_a}{\gamma\sigma_g}. \tag{4.13}$$

Q-Switched Nd:YVO_4

A simple, tunable single-longitudinal mode diode pumped Nd:YVO_4 laser was constructed using a chirped volume Bragg grating (CVBG) as already described in the previous chapter. The laser could be tuned over a large part of the Nd:YVO_4 gain spectrum from 1063 nm to 1065 nm and passive Q-switching using a Cr^{4+}:YAG saturable absorber was obtained both in the low (<20 kHz) and in a high repetition rate (>2 MHz) regime, depending on the operational wavelength chosen with the CVBG.

The tuning and pulsing performance was determined by the center wavelength and the reflectivity of the CVBG aswell as by the gain and the loss in the cavity. At shorter wavelengths, the tuning range was limited by the gain spectrum and towards longer wavelengths, the limit was set by the decreasing reflectivity of the CVBG. As the initial transmission of the Cr^{4+}:YAG saturable absorber was more or less constant over the tuning range, the relation between the gain and the

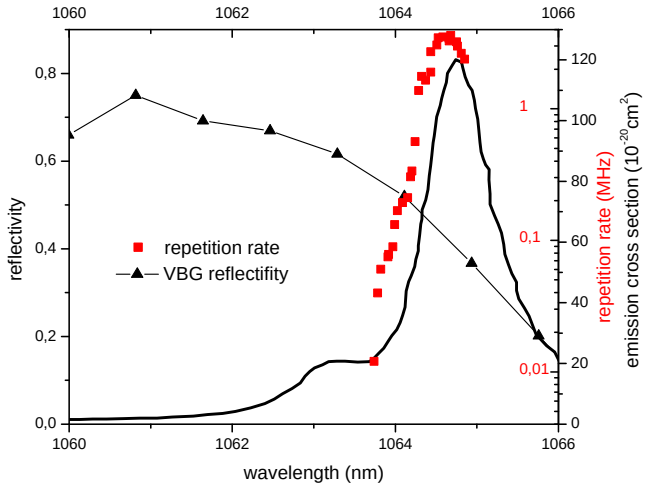

Figure 4.2: Dependence of the repetition rate (logarithmic scale) on the emission cross section (linear scale), and the reflectivity of the CVBG.

additional loss from the out-coupling through the CVBG determined the pulsing behavior.

In Fig. 4.2 the pulse repetition frequency, the CVBG reflectivity and the emission cross section [Cze02] are plotted vs. wavelength. It is clear that the repetition frequency is directly related to the gain and, hence, to the inversion population build-up. As can be seen in the figure, it changes by several orders of magnitude when the laser was tuned over the gain peak. For regions of low gain, i.e. for wavelengths below 1063.7 nm, it takes a longer time to reach threshold and the repetition rate will therefore be low, in this case around 100 kHz. At the same time the inversion becomes high and a large energy can be extracted. When the CVBG was translated and the laser tuned to longer wavelengths, the gain increased and the threshold was reached earlier, resulting in a much higher repetition rate, up to a few MHz, with corresponding low pulse energy. The small difference, < 0.3 nm, between the wavelength of the peak in the emission cross section, as measured by Czeranowsky [Cze02], and our measurement of the wavelength for maximum repetition rate, can very well be explained by the lower reflectivity of the CVBG at longer wavelengths. An important finding in this experiment was that the VBG could force the laser to oscillate in a regime with a low emission cross section around 1063.8 nm, which allowed extraction of high pulse energies from the laser material that otherwise would give low pulse energies.

This experiment is described in more detail in paper II.

4.3 Mode-locking

In contrast to Q-switching, which is possible with a laser running on a single longitudinal mode, mode-locking requires the laser to oscillate on multiple longitudinal modes. The broader the optical spectrum is, the shorter the resulting output pulses can be.
A first description for mode-locked lasers has been made by Martinez [Mar84], based on a model by Haus [Hau75]. The following description is based on the description of Kärtner [Kae04].
The basic principle is that the different longitudinal modes (which of course have a different wavelength/frequency), have a common phase and interfere constructively and oscillate as a single pulse inside the cavity. Such a light pulse can hence be described as a superposition of plane waves with different frequencies, but with the same phase. For a fixed location, the dependence as a function of time can be written as:

$$E(t) = \frac{1}{2\pi}\int_{-\infty}^{\infty}\tilde{E}(\omega)e^{i\omega t}d\omega = \frac{1}{2\pi}\int_{0}^{\infty}\tilde{E}(\omega)e^{i\omega t}d\omega + c.c.. \quad (4.14)$$

In this case, $E(t)$ is the Fourier transform of $\tilde{E}(\omega)$, which is the optical spectrum of the pulse. The abbreviation *c.c.* stands for the complex conjugate. The optical spectrum has a bandwidth of $\Delta\omega$ with a center frequency of ω_0. The shape of the spectrum determines the shape of the pulse.

Typically $\omega_0 \gg \Delta\omega$ and with that, equation 4.14 can be written as follows:

$$E(t) = \frac{1}{2\pi}\int_{-\omega_0}^{\infty}\tilde{E}(\omega_0+\Delta\omega)e^{i(\omega_0+\Delta\omega)t}d\Delta\omega + c.c.. \quad (4.15)$$

This can be further simplified by introducing the envelope function $A(t)$:

$$E(t) = e^{i\omega_0 t}\frac{1}{2\pi}\int_{-\infty}^{\infty}\tilde{A}(\Delta\omega)e^{i\Delta\omega t}d\Delta\omega + const. = A(t)e^{i\omega_0 t} + c.c.. \quad (4.16)$$

$\tilde{A}(\Delta\omega)$ is the frequency shifted, single-sideband spectrum, for which $\tilde{A}(\Delta\omega) = 0$ when $\Delta\omega < -\omega_0$. If $\Delta\omega > -\omega_0$, using equation 4.16, we can now write:

$$\tilde{A}(\Delta\omega) = \tilde{E}(\omega_0+\Delta\omega). \quad (4.17)$$

$A(t)$ is the complex envelope funtion, and with equation 4.16, this leads finally to

$$E(t) = A(t)e^{i\omega_0 t} + c.c., \tag{4.18}$$

and

$$A(t) = \int_{-\infty}^{\infty} \tilde{A}(\Delta\omega)d\Delta\omega. \tag{4.19}$$

A schematic of such a pulse with a Gaussian envelope function can be seen in fig. 4.3.

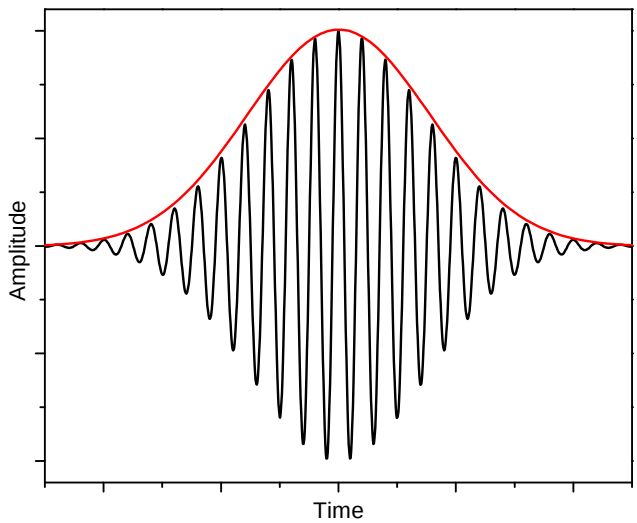

Figure 4.3: Schematic picture of a pulse with a Gaussian envelope function.

The number of elements i inside a typical laser cavity have a small influence on the envelope function and gain and losses are typically only a few percent. The changes are therefore so small, that it does not matter in which order the pulse passes the intracavity elements. So, the total change of the envelope function can be written as:

$$T_R \frac{\partial A(T,t)}{\partial T} = \sum_i \Delta A_i. \tag{4.20}$$

The new time variable T describes the changes on the envelope function for many cavity round trips whereas t describes the time scale of a single pulse. This is the so-called master equation, which can be formulated as [Kra92]:

$$\begin{aligned} T_R \frac{\partial A(T,t)}{\partial T} = & \underbrace{-lA(T,t)}_{\text{linear losses}} + \underbrace{\gamma \left|A(T,t)\right|^2 A(T,t)}_{\text{saturable absorber}} \\ & + \underbrace{\left(g + \frac{g}{\Omega_g^2}\frac{\partial^2}{\partial t^2}\right) A(T,t)}_{\text{gain medium}}. \end{aligned} \tag{4.21}$$

If only mode-locking is present in the laser (no Q-switching instabilities or cw background), we may set:

$$T_R \frac{\partial A(T,t)}{\partial T} = 0. \tag{4.22}$$

This can now be used to calculate the pulse length and the peak intensity for a given pump power if the other laser parameters are known.

Mode-locking can for example be achieved either actively by an external source, or passively, through intracavity saturable absorbers (SA). In this case the focus will be on fast SA mode-locking, since these were exclusively used in this work. Fast, in this context, means that the upper-state lifetime of the SA is short compared to the cavity round-trip time. One major advantage of this is that SA mode-locking is selfstarting from noise. Only very high intensity spikes are able to saturate the SA, so that they will bleach it and some part still pass through. After several round-trips, a complete pulse will be circulating inside the laser cavity and the leading edge of which suffices to bleach the SA and the main part of the pulse is able to pass the SA with only minor losses. A good overview of the theory and history of mode-locking can be found in the excellent review written by Haus [Hau00].

Other passive mode-locking schemes include coupled cavity mode-locking, cascaded mode-locking and Kerr lens mode-locking, but will not be discussed here.

Semiconductor saturable absorber mirrors

Semiconductor saturable absorber mirrors (SESAM) are structures that combine a mirror and a quantum well structure in one component and are used for mode-

locking as a mirror in a laser cavity. The typical SESAM structure provides an intensity dependent variation of the losses:

$$R(I) = 1 - a_0 - \frac{q_0}{1 + \frac{I}{I_{sat}}}. \tag{4.23}$$

The losses in the SA are the sum of the linear (non-saturable) and the nonlinear (saturable) losses. In the semiconductor quantum well, the absorption is dependent on the population of the valence and the conduction band. If photons are being absorbed, electrons are excited from the valence band into the conduction band. The more electrons there are in the conduction band by the absorption of the incident photons, the lower the absorption will become and with that, the reflectivity of the SESAM increases [see picture Niels].

A recent development has been quantum dot SESAMs (QDSESAM), where the quantum wells are replaced by quantum dots (QD). This leads to some unique properties: Large cross-sections of the absorption transitions in the QDs ensure a low absorption saturation fluence and thus give more freedom in the parameter design compared to quantum well structures. This enables for example mode-locking of low-energy solid-state laser systems where a low saturation fluence as well as low modulation depth is necessary to eliminate Q-switching instablilities.

Mode-locked Yb:KYW laser with GHz repetition rate

Fundamental mode-locking of solid-state lasers has been very successful using saturable absorbers based on quantum wells, for a wide range of repetition rates and gain media. Quantum dots (QD) have only been used to achieve high repetition rates with all semiconductor lasers like OPSDL [Hof11] and MIXSEL [Wit12]. Systems based on solid-state crystals have only been mode-locked up to 200MHz and have not been fully investigated the quantum dot absorbers' potential to extend the range to the 1 GHz region. We demonstrated a compact, passively mode-locked Yb:KYW DPSSL operating around 1 GHz repetition rate, taking advantage of the mentioned beneficial properties of the saturable absorber structures containing layers of self-assembled InGaAs quantum dots. This makes such a structure ideal for high-repetition rate mode-locking of a DPSSL with picosecond pulse duration.
The cavity design can be seen in Fig. 4.4. The gain medium is a 3 mm long, 5-at.%-doped, N_g-cut Yb:KYW crystal, pumped by at 980 nm by a collimated stack diode. The QD-SESAM structure hosts three sub-structures, each containing five layers of self-assembled InGaAs quantum dots and 20 nm thick GaAs spacing layers. An anti-resonant design was chosen to minimise the effect of growth errors during production and also to minimise the influence of thermal expansion during operation.

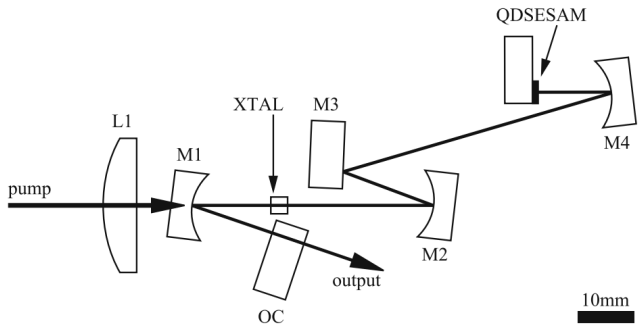

Figure 4.4: Experimental setup of the laser cavity.

The laser directly emited picosecond pulses at center wavelengths around 1035 nm. Reliable CW-mode-locking began at laser output powers of 66 mW, i.e. for a pulse fluence of 165 μJ/cm^2 on the absorber. No Q-switched mode-locking was observed up to the damage threshold of the absorber. The output power in this cavity was limited by the QDSA's damage which occurs at pulse energy fluence of 860 μJ/cm^2.

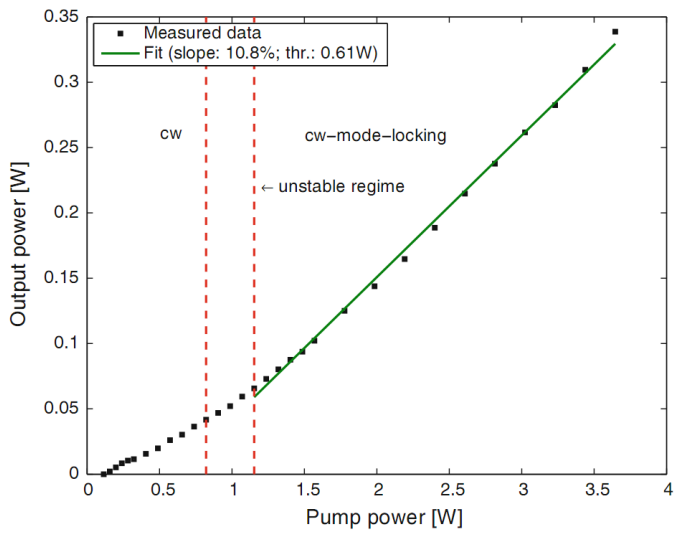

Figure 4.5: Measured output power of the laser, including a division into the different regimes of operation.

This experiment is described in more detail in paper IV.

Single-walled carbon nano tubes

Single-walled carbon nano tubes (SWCNT) are a very interesting type of material with exceptional optical and electrical properties [Iij91]. Their properties are determined by the roll direction (chirality) of the graphene sheet and their diameter. They can show either metallic or semiconducting properties. Especially semiconducting SWCNTs have interesting optical properties such as saturable absorption and a high optical damage threshold.
These forms of SWCNT are usually fabricated by either arc discharge or chemical vapour deposition and commercially available from several companies. They can be purchased with different degrees of purity, limiting the spread of the diameter distribution and the amount of non semiconducting SWCNT.

SWCNTs can be used as saturable absorbers (SWCNT-SAs) and offer a potential alternative for high-gain solid-state laser mode-locking over a wide near-infrared spectral range. Such saturable absorbers can be manufactured on a variety of substrates in a cost-effective way by employing relatively simple techniques such as spray and spin-coating [Yim08]. Moreover, they possess broadband ultrafast saturable absorption behaviour and the samples can be used in reflection or transmission.
A good overview of the fabrication and characterization of SWCNT as well as their use in mode-locked lasers near 1 μm can be found in [Rot12].

The samples used in this work were prepared in a multi-stage process (see fig. 4.6): First the CNTs were dissolved in 1,2-dichloro benzene at a concentration of 0.2 mg/ml. To improve the dissolving, the surfactant PmPV, with a concentration of 5 mg/ml was added and the solution centrifuged for 30 minutes and only the upper third was used in the following process. At the same time, PMMA was dissolved in 1,2-dichloro benzene with a concentration of 100 mg/ml. Both solutions are added together at a 1:1 ratio and after stirring the solution for 12 hours, spin-coated onto a one millimeter thick glass window.

Mode-locked OPSDL using SWCNT

It is not obvious that a SWCNT-SAs can be employed for mode-locking OPSDLs due to low roundtrip gain and large nonsaturable absorption loss in a typical SWCNT-SAs reported previously. We have demonstrated, that saturable absorbers based on SWCNTs with low loss operating in transmission can be used for mode-locking an OPSDL. Stable fundamental mode-locking was obtained for such a system generating 1.23 ps pulses at a repetition rate of 613 MHz, delivering output powers of up to 136 mW near 1074 nm. The laser setup represents a highly practi-

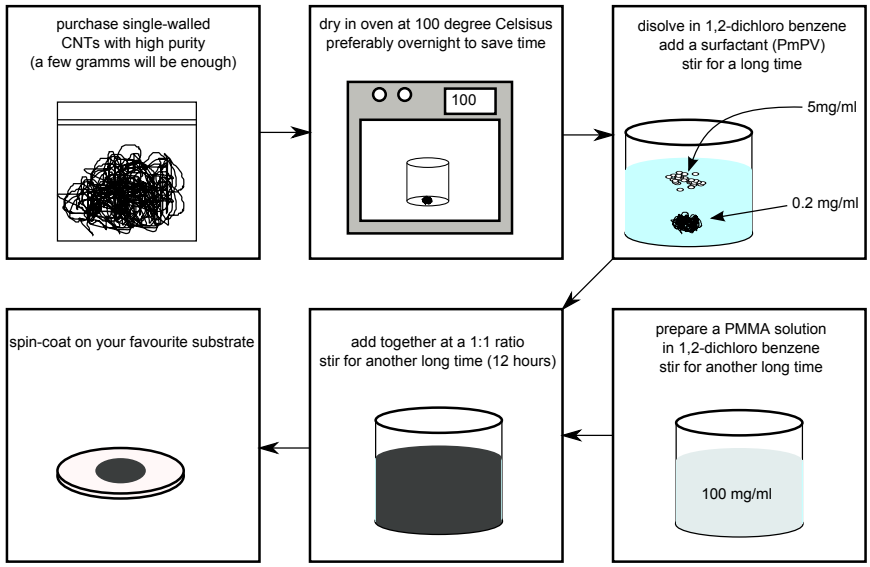

Figure 4.6: Preparation steps of SWCNT-SA samples.

cal and simple solution for a high-repetition rate solid-state laser operating in the near-infrared spectral region. This first application of a SWCNT-SAs for mode-locking of an OPSDL represents an important step for a further enhancement of the versatility of both devices and can be seen as an alternative, easy to implement and cost effective design.

In the experiment we employed a V-type cavity with a total length of about 244.5 mm (see Fig. 4.7). The cavity consisted of the gain structure in the first beam waist and the SWCNT-SA for mode-locking was placed in the second beam waist. The gain structure was angle-pumped by a fiber coupled laser diode at 808 nm. A SWCNT-SA was inserted at Brewster's angle, fabricated as mentioned above. The fabricated SWCNT-SAs were characterized by linear and nonlinear transmission measurements (see Fig. 4.8). The modulation depth of the SWCNT-SA used was measured to be 0.25 % and the saturation fluence (F_{sat}) 11.36 μJ/cm^2 with non-saturable losses of about 1 %.

This experiment is described in more detail in paper VII.

Q-Switching using SWCNT

Recently Q-switching using single-walled carbon nano tubes has been presented in a Nd:LuYGdVO$_4$ laser [Che11] and in a Nd:YAG ceramic laser [Li12]. Furthermore Qin et. al. [Qin11] reported on a Nd:YVO$_4$ laser with 332 ns long pulses at a pulse

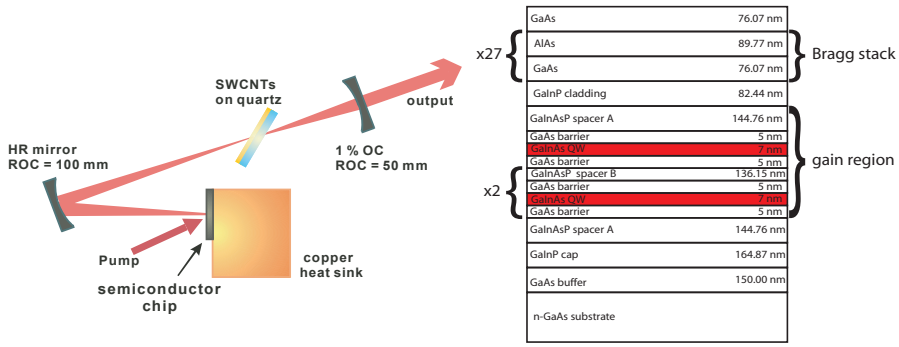

Figure 4.7: Experimental Setup of the laser cavity and the layout of the OPS gain-chip structure.

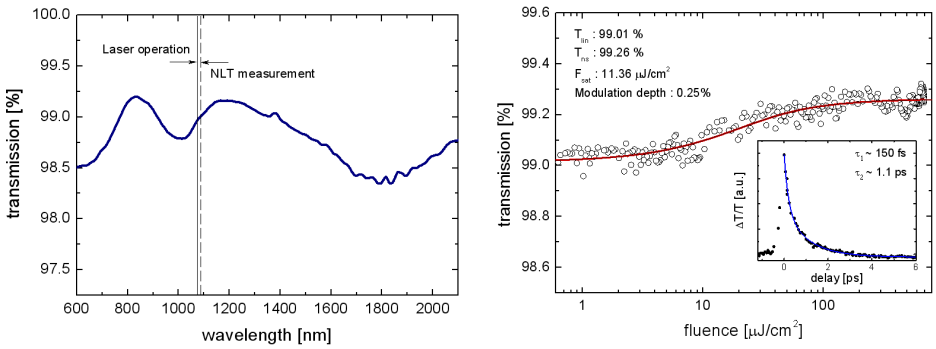

Figure 4.8: SWCNT parameters.

energy of 326 nJ and observed mode-locking instabilities, however essential details like the modulation depth of their absorber samples have not been presented.
Here, an alternative absorber based on SWCNT with substantially lower saturable and non-saturable losses is presented. Although this type of SWCNT absorber is most commonly used for passive mode-locking due to the excellent performance with regard to its transient absorption behaviour [Set04], [Cho10], we show, that the high mode coherence instabilities can be suppressed by the use of a spectrally limiting VBG written in thermo-refractive glass [Efi99]. The laser can thus be driven with high slope efficiency and clean Q-switch pulses. We also provide data on the SWCNT samples used as well as an analysis of the output pulse parameters.

The laser cavity featured a simple, linear design with the VBG as the input coupler and a curved mirror as the output coupler (see fig.4.9). The VBG (2x2x1.5 mm^3) was anti-reflection coated for both the pump wavelength of 808 nm and the laser wavelength at 1064 nm. The peak reflectivity was 97.5 % with a bandwidth of 0.5 nm at 1063.6 nm. The output coupler had a reflectivity of 95 %, a radius of curvature of 100 mm and it was placed at a distance of 80 mm from the VBG. A 0.7 % at. doped Nd:YAG with dimensions of 3x3x3 mm^3 was used as the gain medium for the laser and was as well anti reflection coated for both the pump wavelength of 808 nm and the laser wavelength of 1064 nm. It was pumped by a fiber-coupled 808 nm laser diode, which was focused into the laser crystal with a spot size of 110 μm ($1/e^2$ radius). A SWCNT-SA plate at Brewster's angle was inserted into the centre of the cavity. The SWCNT-SA sample was the same used in the above explained experiment.

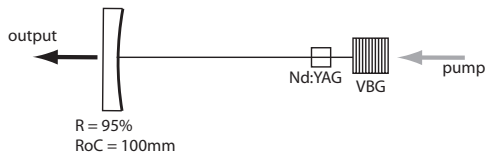

Figure 4.9: Experimental Setup of the laser cavity.

In order to evaluate the performance of the laser, we measured the average power, pulse width and repetition rate for different incident pump powers as can be seen in fig. 4.10. At the highest pump power of 10.9 W, the pulses had a temporal bandwidth of 417 ns at a repetition rate of 345 kHz at an average power of 1.16 W. This corresponds to pulses with a peak power of 7.41 W and a pulse energy of 3.34 μJ. The fluence on the SWCNT-sample is $212\mu J/cm^2$ and with that 18-times higher (than F_{sat}) than the well known Q-switched mode locking threshold $E_p^2 > E_{sat,g}E_{sat,a}\Delta R$ [Hoe99].
The pulse length is rather long with 417 ns as a Q-switched Nd:YAG using saturable absorbers typically emits pulses with a pulse length of a few nanoseconds. For that reason, the experimental result should be compared to a theoretically expected value. For a fast Q-switch, the pulse length can be estimated with [Koe06]:

$$t_p = \frac{t_r}{\delta}\left(\frac{\ln(z)}{z\,(1-a(1-\ln a))}\right) \tag{4.24}$$

with t_r as the round-trip time, δ as the round-trip losses and $a = (z-1)/(z\ln(z))$. In this case, the parameter $z = 2g_0l\delta$ is the logarithmic small signal gain divided by the resonator losses. The small signal gain can be hard to measure and another solution is more accessible: As the output energy E_{out} was measured, the following relation can be used to calculate the z-parameter [Koe06]:

$$E_{out} \quad = \quad E_{sc}\,(z - 1 - \ln(z)) \tag{4.25}$$

The energy E_{sc} is defined by $E_{sc} = Ah\nu\delta/2\sigma\gamma$, A is the beam cross section in the laser crystal, $h\nu$ is the laser photon energy, σ is the stimulated emission cross section of the laser transition and γ is one for a four-level laser. Those parameters are easily obtainable and with that equation 4.25 is solvable numerically and with that the estimated pulse length t_p can be calculated to 310 ps. The reason the pulse length is rather long is the comparably low stimulated emission cross section of $2 \cdot 10^{-20}$ J/cm^2 at the laser wavelength, since the laser is VBG-locked at 1063.83 nm, where the gain is an order of magnitude lower compared to the main peak of the stimulated emission cross section.

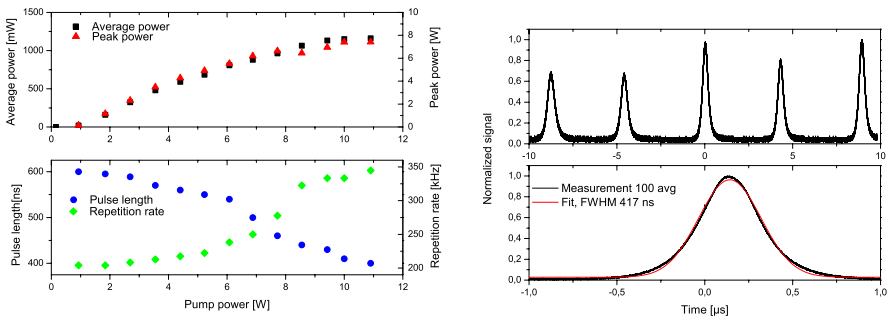

(a) Output power and change of the temporal characteristics with time.

(b) Oscilloscope trace of the pulse train.

Figure 4.10: Performance of the Laser.

If the VBG was replaced with a dielectric input coupling mirror, instabilities could be observed and no stable Q-switching could be achieved. Figure 4.11 shows a typical trace for the observed instabilities at an intermediate pump power of 8 W. In the first figure one can clearly see, that there is a modulation on the pulse. However, the pulses are not stable and one can often observe transitions between continuous wave behaviour with a fast modulation to Q-switching with a fast modulation on top. The modulation is probably associated with a high phase coherency or could also be Q-switched mode-locking.

The output spectrum was measured with an optical spectrum analyzer with a resolution bandwidth of 0.05 nm (see Fig. 4.12. The spectrum was centered around $\lambda_c = 1063.83$ nm with a bandwidth $\Delta\lambda_{FWHM} = 0.59$ nm. The spectrum seems to be slightly red-shifted by 0.3 nm from the main peak of the VBG reflectivity

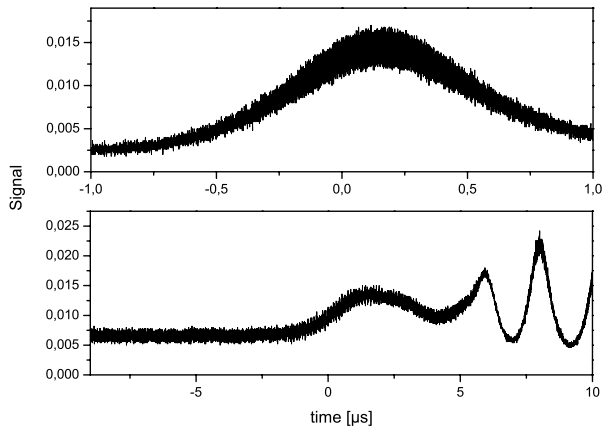

Figure 4.11: Typical traces for instabilities occuring with a dielectric input coupler instead of the VBG.

curve. However, the reflectivity of the VBG was measured with a continous wave Ti:Saphire laser at low power (see fig. 4.12). The cause of the red-shift is heating of the VBG by the incident pump and the laser radiation, which results in a small thermal expansion and a change in the Bragg condition and a red-shift of the spectrum. The beam propagation factor $M^2 = 1.3$ was measured using the knife-edge-method.

With this system, pulses as short as 417 ns with a pulse energy of 3.34 μJ were measured. This demonstrates, that SWCNT absorbers with a low modulation depth of only 0.25 % can be used for efficient and stable Q-switching.
As SWCNT can be used over a broad range in the near-infrared spectral region, this new method to achieve stable Q-switching with SWCNT saturable absorbers with low modulation depth is transferable to other solid-state laser systems as well and provide route to inexpensive mass fabrication of passively Q-switched lasers. Further improvement could be done by matching the VBG wavelength under operation better to the main stimulated emission cross section peak in order to achieve even shorter pulses and higher average output power.

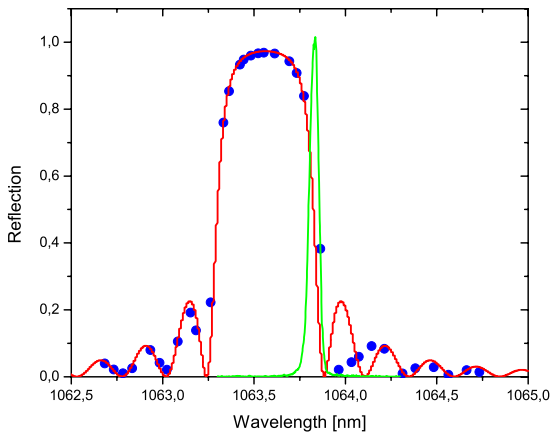

Figure 4.12: Measured reflectivity of the VBG using a Ti:Saphire laser at low power and output spectrum of the laser at maxium output power. The red-shift of the output spectrum is a result from laser and pump radiation heating the VBG.

5

Second Harmonic Generation

In this chapter, the basics of nonlinear optics are introduced, focussing on second-harmonic generation. This is followed by an overview of the experiments linked to nonlinear optics.

5.1 Basic theory

For the propagation of light in matter in a nonlinear optical medium, we will apply the fundamental principles of superposition and frequency conversion [Ber04]. The description of the effects in nonlinear optics is carried out using the index of refraction and the absorption in the medium as material parameters. The intensity of the incident light is usually small compared to the inner atomic fields and thus the polarization $\mathbf{P}$[1] of the medium is linear dependent on the field strength $\mathbf{E}$ of the incident light:

$$\mathbf{P}(\mathbf{r},t) \quad = \quad \epsilon_0 \chi^{(1)} \mathbf{E}(\mathbf{r},t) \tag{5.1}$$

Here, we have used the frequency dependent dielectrical susceptibility $\chi^{(1)}$, which is a second-order tensor. From this we can define the dielectric tensor ϵ_{ij} in an isotropic media (ϵ_0 is the dielectric constant in vacuum):

$$\epsilon_{ij} \quad = \quad \epsilon_0 \chi_{ij}^{(1)} + \delta_{ij} \qquad i,j \in \{1,2,3\}. \tag{5.2}$$

With this, one can describe the dielectric deplacement $\mathbf{D}$, which is well known from the Maxwell-equations:

$$\mathbf{D} \quad = \quad \epsilon \mathbf{E}. \tag{5.3}$$

[1] Vectors and tensors will be written in bold letters.

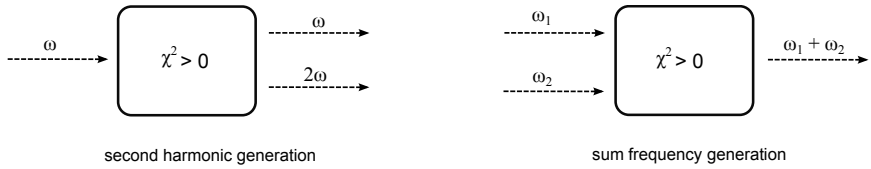

Figure 5.1: SHG and SFG.

In the case of linear optics, it is possible to describe well-known optical phenomena such as absorption, reflection and refraction. Details can be found in [Hec98] for example.
However, the intensity of laser light is often quite high, so that the polarization of the medium cannot be seen as linearly dependent of the incident intensity. The polarization has to be developed in a power series, adding nonlinear terms. In component notation, the polarization can be written in the following way:

$$P_i = \epsilon_0 \chi_{ij}^{(1)} E_j + \epsilon_0 \chi_{ijk}^{(2)} E_j E_k + \epsilon_0 \chi_{ijkl}^{(3)} E_j E_k E_l + ... \tag{5.4}$$

Through the higher-order terms, new effects are appearing, which can be described in terms of nonlinear optics. One of those is the second harmonic generation.

Second harmonic generation

The second-order term in equation 5.4 is responsible for the two cases of second harmonic generation and sum frequency generation. If two electromagnetic waves of frequencies ω_1 and ω_2 are superimposed in a nonlinear medium, the polarization can now be written as a sum (here, only the terms until the second order are included):

$$\begin{aligned} \mathbf{P} = {} & \mathbf{P}^{(1,1)}(\omega_1) + \mathbf{P}^{(1,2)}(\omega_2) + \mathbf{P}^{(2,0)} \\ & + \mathbf{P}^{(2,+)}(\omega_1 + \omega_2) + \mathbf{P}^{(2,-)}(|\omega_1 - \omega_2|) + \mathbf{P}^{(2,1)}(2\omega_1) + \mathbf{P}^{(2,2)}(2\omega_2)... \ . \end{aligned} \tag{5.5}$$

The $\mathbf{P}^{(1)}$-terms result from the linear susceptibility $\chi^{(1)}$, and the $\mathbf{P}^{(2)}$-terms likewise from the nonlinear susceptibility $\chi^{(2)}$.

This polarization wave generates electromagnetic waves in the nonlinear medium, which, of course, contains both the fundamental frequencies ω_1 and ω_2 and the generated doubled frequencies $2\omega_1$ and $2\omega_2$, as well as the sum $(\omega_1 + \omega_2)$ and the difference $(|\omega_1 - \omega_2|)$ of the two fundamental frequencies (see fig. 5.1). In a laser which is oscillating on several longitudinal modes, the SHG and SFG often have a temporal and spatial overlap and the SFG can lead to a coupling of the fundamental frequencies [Bae86]. This can fundamentally influence the output dynamic of a laser and lead to large amplitude fluctuations, which will be discussed later.

Phasematching

The fundamental field of frequency ω together with the second harmonic field of frequency 2ω, which is generated in the nonlinear medium, will experience a different index of refraction and thus the phase difference changes due to different velocities. When the SH wave has accumulated a phase mismatch of $\frac{\lambda}{4} < \triangle\varphi < \frac{3\lambda}{4}$, there will be destructive interference and as a result the backconversion of the second harmonic. The distance, where the phase mismatch is $\frac{\lambda}{2}$, is called the coherence length L_c, defined as:

$$L_c = \frac{\lambda}{4(n_1 - n_2)}. \tag{5.6}$$

This reduction of the second harmonic field is the equivalent of a back-conversion to the fundamental wave because of the conservation of energy. Only through phase-matching of the two wave vectors $\mathbf{k}_\omega$ and $\mathbf{k}_{2\omega}$ with the condition that

$$\triangle\mathbf{k} = 2\mathbf{k}_\omega - \mathbf{k}_{2\omega} = 0, \tag{5.7}$$

we ensure that a phase-matching over a length longer than the coherence length L_c is possible (see fig. 5.2).

Birefringent phase matching

One possible way to achieve phase matching is to use the built-in natural birefringence of optically anisotropic crystals, because in that case the polarization-dependant index of refraction is different for different propagation directions. For an uniaxial crystal, the indices of refractions are called the ordinary refractive index n_o (lowest or highest index of refraction) and the extraordinary refractive index n_e (index of refraction for perpendicular to n_o polarized wave). One can then choose an angle θ of the wave vector $\mathbf{k}_\omega$ in relation to the optical axis, so that:

$$n_{o,\omega} = n_{e,2\omega}(\theta). \tag{5.8}$$

With that, phase matching is achieved and there is no dispersion between the fundamental and the second harmonic fields. The angle θ is given by

$$\frac{1}{n^2_{e,2\omega}(\theta)} = \frac{\cos^2(\theta)}{n^2_{o,2\omega}} + \frac{\sin^2(\theta)}{n^2_{e,2\omega}}. \tag{5.9}$$

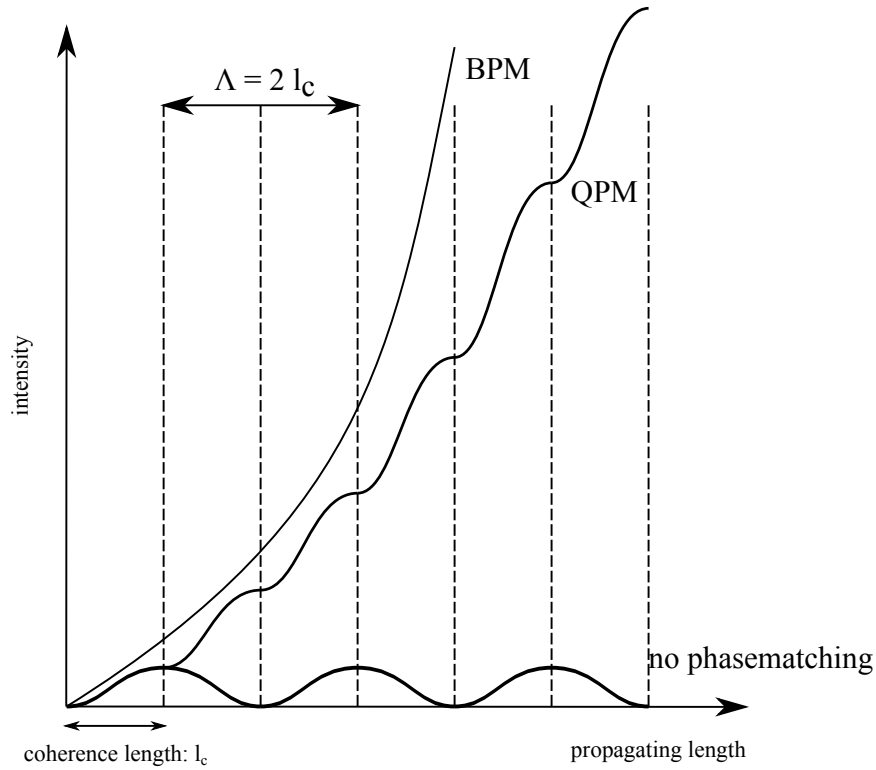

Figure 5.2: Power of the SHG in dependence of the number of the coherence length l_c.

Quasi phase matching

Another possibility for achieving phase matching is to engineer the nonlinear coefficient periodically in a way so that the accumulated phase difference between the fundamental and second harmonic fields is reset. This is called quasi-phase-matching (QPM) and the wave vector mismatch can be written as:

$$\Delta\mathbf{k}_Q \quad = \quad \mathbf{k}_{2\omega} - 2\mathbf{k}_\omega - \mathbf{k}_G. \tag{5.10}$$

with $\mathbf{k}_G$ as the wave vector of the periodic grating, whose absolute value is given by:

$$|\mathbf{k}_G| = m\frac{2\pi}{\Lambda}. \tag{5.11}$$

In this equation, Λ is the period of the grating and its value is of the order of twice the coherence length of the interacting waves. The effective nonlinear coefficient d_{eff} is reduced by the Fourier amplitude of the m-th spatial harmonic of this modulation:

$$d_{eff} = \frac{2}{m\pi} d_{ij}. \tag{5.12}$$

This might seem to be a drawback, but the QPM technique enables noncritical phase matching within the transparency range of the employed crystal. In this way, the highest nonlinearity d_{ij} can be used independent of the wavelength. A more detailed description can be found in [Wan05].

Internal second-harmonic generation

In order to achieve a high conversion efficiency, high intensities are needed as the generated second-harmonic intensity scales with the square of the incident fundamental intensity. For cw lasers, this can be achieved by placing the nonlinear medium inside the laser cavity, where the intensity of the fundamental is much higher than outside. For the highest intensity, the cavity mirrors have to be highly reflective for the fundamental frequency, and the out coupling mirror has to be highly transmissive for the second harmonic frequency. As the second harmonic field is not resonating, the out coupling can be as high as possible.
The intensity of the second harmonic $I_{2\omega}$ that is generated for a double-pass in the nonlinear medium can be written as:

$$I_{2\omega} = 2KI^2. \tag{5.13}$$

where K is the nonlinear coupling constant and I the incident fundamental intensity. The generation of the second harmonic intensity $2KI^2$ can be considered a loss for the laser in addition to the other present losses γ. These losses have to be compensated by the gain $\frac{2g_0\,l}{1+\frac{I}{I_s}}$ so that the laser can operate. Because of that, we can now write:

$$\frac{2g_0\,l}{1+\frac{I}{I_s}} = \gamma + 2KI^2, \tag{5.14}$$

in which g_0 is the small-signal gain $g_0 = \sigma_{SE}(N_2 - N_1)$ and the saturation intensity is given by $I_s = h\nu_L/\sigma_{SE}\,\tau$. From that, we obtain a condition for the optimal nonlinear coupling:

$$K_{opt} = \frac{\gamma}{I_s}. \tag{5.15}$$

Now we can write the equation 5.13 as follows:

$$I_{2\omega,opt} = 4g_0 l I_s \left(1 - \sqrt{\frac{\gamma}{2g_0 l}}\right)^2. \tag{5.16}$$

The output of the intracavity, second harmonic generation can suffer from large periodic or chaotic amplitude fluctuations. This phenomenon is known as the "green-problem", since it was first observed for frequency doubling into the green spectral range [Bae86].
Baer has described the green problem both experimentally and theoretically using a Nd:YAG laser with an intracavity KTP (potassiumtitanylphosphat, $KTiOPO_4$) nonlinear crystal for second harmonic generation. He used a set of $2N$ coupled differential equations for the laser, which was oscillating on N longitudinal modes. Equation 5.17 below describes the intensity change of the i-th mode and equation 5.18 the gain of the i-th mode, respectively:

$$\tau_c \frac{dI_i}{dt} = \left(G_i - \alpha_i - \epsilon I_i - 2\sum_{j\neq i}^{N} \epsilon I_j\right) I_i, \tag{5.17}$$

$$\tau_f \frac{dG_i}{dt} = -\left(\beta I_i + \sum_{j\neq i}^{N} \beta_{ij} I_j + 1\right) G_i + G_i^0. \tag{5.18}$$

In comparison to the rate equations of a 4-level-systems (see chapter 2), the losses of the intensity of the i-th mode through frequency doubling $-\epsilon I_i$ and the sum frequency generation $-2\sum_{j\neq i}^{N} \epsilon I_j$ are added. The term $\sum_{j\neq i}^{N} \beta_{ij} I_j$ couples the gain of the i-th mode to the intensity of the j-th mode, so that the cross saturation of the two modes is included. This describes the spatial and the spectral overlap of the modes in the gain medium as well as in the nonlinear crystal. Table 5.1 describes the other parameters and gives the numeral values assumed by Baer:

parameter	description	Nd:YAG
β_{ij}	cross-saturation of the modes i and j	0,666 W^{-1}
τ_c	cavity round-trip time	0,5 ns
τ_f	fluorescence-lifetime	0,24 ms
α_i	losses of the mode i	0,015
ϵ	nonlinearer coupling coefficient	$5{\cdot}10^{-5}$ W^{-1}
β	saturation parameter	1 W^{-1}
G_i^0	small signal gain	0,12

Table 5.1: Parameters for the frequency doubling model described by Baer.

The results of this model are in good agreement with the observed behaviour of the Nd:YAG laser described by Baer:

- A laser oscillating on one mode is stable.
- A laser oscillating on two modes shows periodic fluctuations.
- A laser oscillating on three or more modes shows chaotic fluctuations.
- For a decreasing nonlinear coupling coefficient, the frequency of the fluctuations will increase up to the relaxation frequency of the laser. Above that, the laser is stable.
- The frequency of the fluctuations is typically in the kilohertz range and not dependent from the pump rate.

External second harmonic generation

Efficient SHG outside of the laser cavity can be achieved with either very high power cw lasers or with pulsed lasers, as the peak power of the latter often is orders of magnitude higher than the average power.
The theoretical value of the generated second-harmonic power (P_{SH}) can be calculated assuming a temporally Gaussian-shaped input pulse and optimal focussing. For high conversion efficiency, the pump depletion must be taken into account. The theoretical value can be expressed as [Yar89]:

$$\eta_{SH} = \frac{P_{SH}}{P_F} = \tanh^2\left[\left(\gamma'_{SH} P_F\right)^{1/2}\right]. \tag{5.19}$$

Here, P_{SH} and P_F are the average power of the the second harmonic and fundamental, respectively, and γ'_{SH} is the nonlinear coefficient for short pulses. In this case, the group-velocity dispersion and self-phase modulation are neglected. γ'_{SH} is then defined as [But95]:

$$\gamma'_{SH} = \gamma_{SH}\left[\left(\frac{2\ln 2}{\pi}\right)^{1/2}\right]\frac{1}{\tau f}. \tag{5.20}$$

The input pulse is characterized by its full width at half maximum pulse duration τ and the pulse train has a repetition rate of f. The nonlinear coefficient γ_{SH} without pump depletion and with a continuous wave fundamental is defined as:

$$\gamma_{SH} = \eta_{norm} L_{eff} = \frac{P_{SH}}{P_F^2 L_{eff}} L. \tag{5.21}$$

In this equation, $\gamma_{SH} = \eta_{norm} L_{eff}$ is the nonlinear coefficient for the continuous wave case without pump depletion [Boy68], with L_{eff} as the effective length of the employed nonlinear crystal.

As an example, these results have been used to calculate the conversion efficiency for a PPKTP crystal with a length of 1mm, 2mm and 3mm using a mode-locked

laser at 975 nm. The important parameters of the laser used in the simulation and the experiment are:

parameter	description	size
λ	wavelength	975 nm
$\Delta\lambda$	spectral bandwidth	1.62 nm
τ	pulse width	1.5 ps
f	repetition rate	500 MHz

Table 5.2: Parameters for the simulation.

However, this does not take into account that the acceptance bandwidth becomes smaller, the longer the crystal length L of the PPKTP is. This limits the amount of the fundamental power that can be used to generate the second harmonic wave [Fej92]:

$$\Delta\lambda_{FWHM} = \frac{0.4429\lambda}{L}\left|\frac{n_{SH-n_f}}{\lambda} + \frac{\partial n_F}{\partial\lambda} - \frac{1}{2}\frac{\partial n_{SH}}{\partial\lambda}\right|^{-1}. \tag{5.22}$$

This has to be taken into account for the simulation. The results are shown in fig. 5.3.

In order to confirm the results of the simulation, an experiment with a PPKTP crystal was performed, the parameters are as follows. For the experiment, the PPKTP crystal was placed on a temperature controlled heatsink and the laser was focused into the middle of the crystal using a lens with a focal length $f = 40$ mm, creating a beam waist of 40 μm.

parameter	description	size
Λ	grating period	6.67 μm
L_{eff}	effective length	15.1 mm
d_{eff}	effective nonlinearity	9.59 pm/V
T	temperature	102 °C

Table 5.3: Experimental parameters.

This shows, that the used simulation is in reasonably good agreement with the experiments. In order to get higher conversion efficiency, shorter crystals in the range of 1 mm to 3 mm should be used.

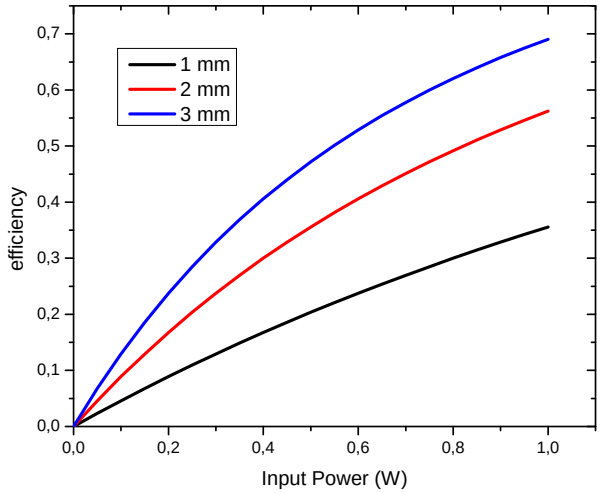

Figure 5.3: Calculated conversion efficiency in dependence of the fundamental input power.

Periodically poled KTP

For the second harmonic generation experiments performed for this project, periodically poled potassium titanyl phosphate (PPKTP) was used for type I noncritical quasi phase-matching. KTP has favorable properties for periodic poling, since it is a nonlinear ferroelectric crystal with a low coercive field. In addition KTP has a wide transparency range and a relatively high damage threshold.

Periodic poling is achieved by engineering the domain structure of ferroelectric nonlinear crystals. They are fabricated in the following process: First, a photoresist is spun onto the KTP crystals, and using photolithography the desired pattern is created. Then an electrode is deposited on top of it, allowing to contact an external circuit in order to apply high voltage electric pulses above the coercive field strength. These electric pulses will change the domain orientation and subsequently, a QPM structure is formed (see [Can05] for more details).

A PPKTP crystal should be characterized in the low-power continuous wave regime using a laser which is adjusted to a moderate and stable output power at the fundamental wavelength. In order to quantize the performance of a periodically-poled, nonlinear crystal, the effective length L_{eff} and effective nonlinearity d_{eff}

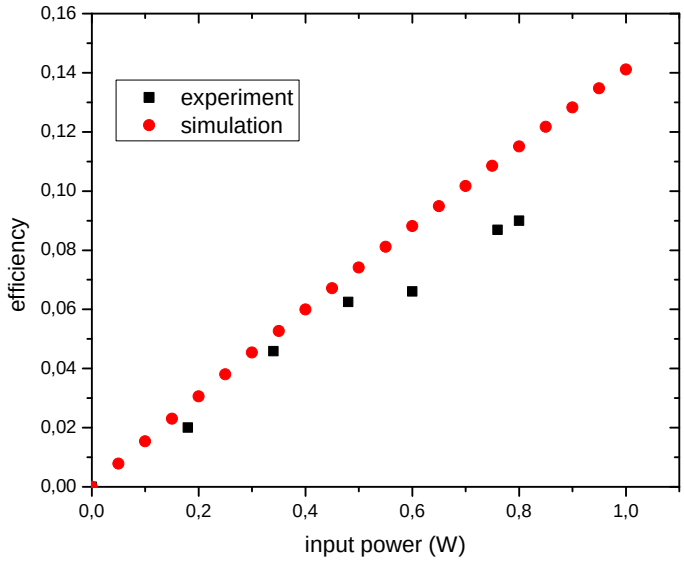

Figure 5.4: Results of the simulation (red dots) and measured efficieny (black squares).

have to be measured. The PPKTP crystal has to be placed on a holder which allows a smooth temperature tuning. The laser has to be focused into the centre of the PPKTP crystal. For a fixed pump wavelength, the temperature acceptance bandwidth can be written as [**?**]:

$$\Delta T_{FWHM} = \frac{0.4429\lambda_F}{L_{eff}} \left[\left.\frac{\partial n_{SH}}{\partial T}\right|_{T_0} - \left.\frac{\partial n_F}{\partial T}\right|_{T_0} + \alpha\,(n_{SH} - n_F) \right]^{-1}, \qquad (5.23)$$

By measuring ΔT_{FWHM} (see Fig. 5.5) and using the material parameters, the thermal expansion coefficient α [Bie89], and the derivatives of the refractive indices (n_{SH} at the second harmonic and n_F at the fundamental wavelength) one can calculate the effective length of the crystal. From the sinc^2 fit to the measured data we calculated a temperature acceptance bandwidth of ΔT_{FWHM} of 5 °C, which results in an effetive length L_{eff} of 2.99 mm, which is close to the PPRKTP crystal's physical length of 3.2 mm.
From the same measurement, it is possible to derive the effective nonlinearity d_{eff} by measuring P_{SH}, the power of the SHG, at 514.5 nm P_{SH}, the input power of

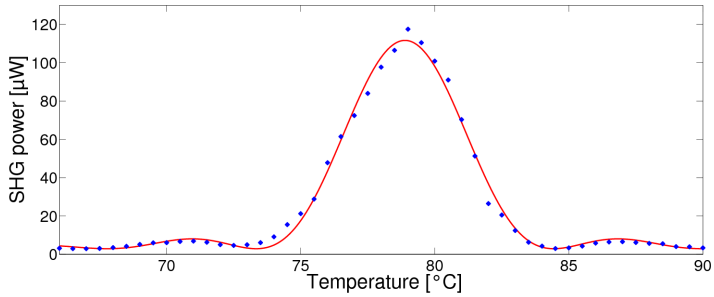

Figure 5.5: Temperature tuning curve of the PPKTP with a sinc^2 fit.

the fundamental at 1029 nm P_F and the focussing condition through the Boyd-Kleinmann factor $h(B,\xi)$ [Boy68] as given by the following expression of:

$$\eta_{norm} = \frac{P_{SH}}{P_F} = \left(\frac{2\omega_F^2 d_{eff}^2 k_F P_F}{\pi n_F^2 n_{SH} \epsilon_0 c^3} \right) L_{eff} \cdot h(B,\xi) . \tag{5.24}$$

From this, a d_{eff} of 10.4 pm/V is obtained which is very close to the theoretical value of $d_{eff} = 2d_{33}/\pi = 10.8$ pm/V [Van92].

5.2 SHG experiments

Yb:KYW laser with intracavity SHG

The laser is the same Yb:KYW laser at 1029 nm as already demonstrated in chapter 3, using a VBG as the input coupler. A Rb-doped PPKTP crystal (PPRKTP) was inserted in the second beam waist in the V-shaped cavity, between two mirrors M_1 and M_2, on a temperature controlled copper heatsink which was kept at 80 °C. A maximum green power of almost 1.1 W was obtained for 17 W of pump power, as can be seen in Fig. 5.6. The linewidth at 514.5 nm was measured to be smaller than 0.05 nm, limited by the resolution of the spectrum analyzer. The green output power was almost as high as that which was obtained in the IR. This corresponds to a large depletion of the IR radiation. The conversion efficiency in case of a partially depleted fundamental beam is described by [Yar89]:

$$\eta_{SH} = \frac{P_{SH}}{P_F} = \tanh^2 \left[(\gamma_{SH} P_F)^{1/2} \right] , \tag{5.25}$$

where P_F and P_{SHG} are the intracavity fundamental and the generated second-harmonic powers, respectively. Here $\gamma_{SH} = \eta_{norm} L_{eff}$ is the nonlinear coefficient for the continuous wave case without pump depletion [Boy68] with $\eta_{norm} =$

$P_{SH}/\left(P_F^2 L\right)$. To calculate the expected power of the SH, knowledge of the IC power is needed. It can be derived from the total average output power and the total loss (transmission of the mirrors and additional internal loss) without SHG. Together with the relevant nonlinear material parameters (L_{eff} and d_{eff}) the nonlinear conversion is known and the depletion at a certain pump power can be determined. It is then possible to fit the curve to the measurement by using the laser threshold, i.e. generation of SH, as the starting point for the simulation, see Fig. 5.6. It can be seen that the SH power curve follows the theoretical calculation until just below 1 W of green light is generated. At that point the IC fundamental power clamps at a level of 16 W and a further increase in pump power just leads to leakage of fundamental radiation out through the VBG. The M^2 beam propagation factor of the SHG was measured to be 1.3. The green output power was stable and had peak to peak fluctuations below 1.5 %.

A more detailed description of this experiment can be found in paper VI.

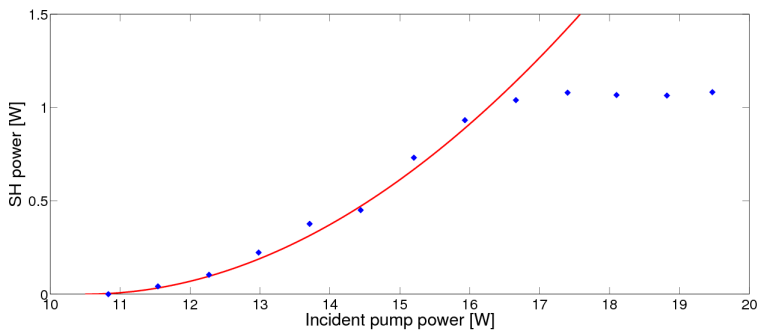

Figure 5.6: Measured output power for the SHG (dots) and theoretical prediction (solid line).

OPSDL green problem

The green problem for solid state lasers can be described by the model introduced by Baer [Bae86] as mentioned earlier, however it is not possible to describe the behavior of an intracavity frequency-doubled OPSDL with this model. The strength of the coupling and therefor the strength of the amplitude fluctuations depends strongly on the fluorescence lifetime. As the fluorescence lifetime is much shorter in VECSEL (∼ns), than in solid-state laser (∼ms), no amplitude fluctuations should occur. Inserting a frequency doubling crystal in the laser cavity, the green problem could be observed under certain conditions.

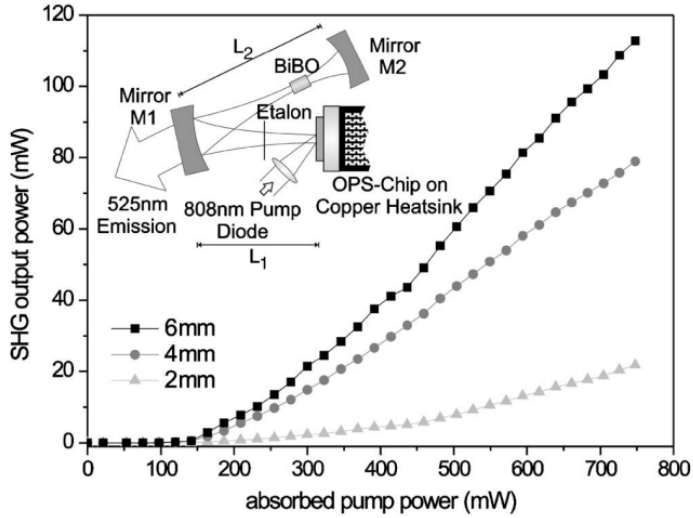

Figure 5.7: Measured output power of the second harmonic for different lengths of the BiBO nonlinear crystal. the inset shows the experimental setup.

In order to investigate this behaviour, an optically-pumped semiconductor disk-laser at 1050 nm, using BiBO for intracavity frequency-douling, was constructed (see Fig. 5.7). The laser typically emits stable output for the second harmonic, which can be explained by the tendency for single-mode operation. The reason for a single-mode operation is the nearly ideal homogeneous gain broadening where adjacent modes seize the same spatial inversion distribution. However, even if two adjacent modes are oscillating at the same time, which can be the case for longer cavities, no green problem was observed. We attribute this to a strong gain coupling of the modes, i.e., both modes see almost the same spectral gain and spatial gain distribution.

To examine the dependence of the output dynamics on the gain-decoupling of laser modes, etalons of different thicknesses were used to vary the gap between the two fundamental wavelengths. The optical spectrum was recorded and the amplitude noise measured at the same time (see Fig. 5.8). In these spectra, the outer peaks result from SHG and middle peak can be attributed to SFG. The presence of the SFG component indicates that two infrared wavelengths were oscillating simultaneously. It can be seen that the green problem comes up if the OPS disk laser is forced to dual-wavelength operation at larger wavelength separation. The gain decoupling of the two laser modes due to spatial inhomogeneity increases with the

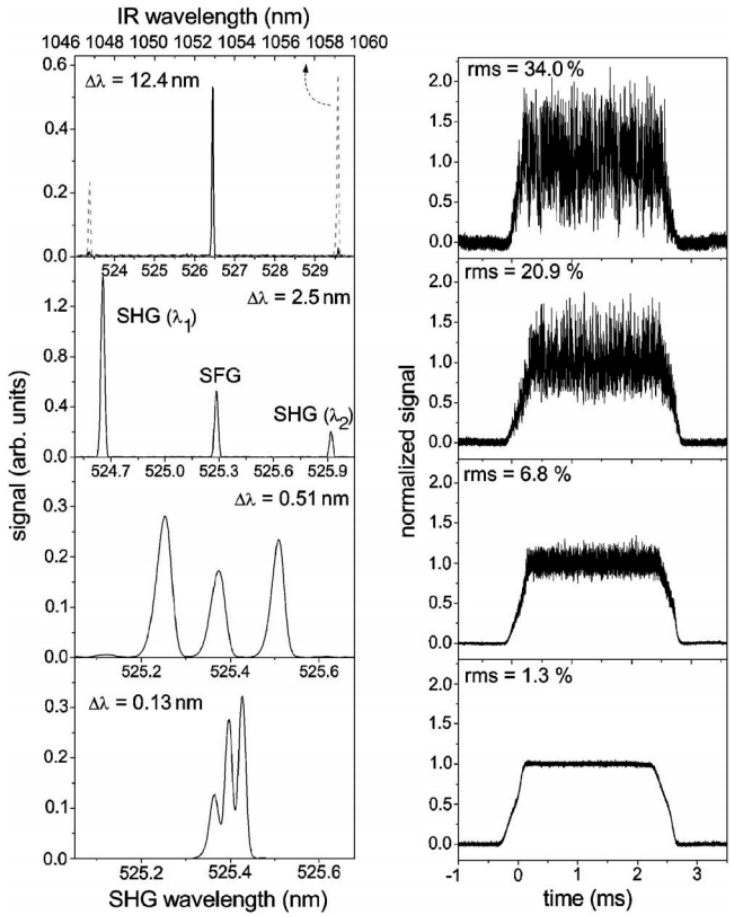

Figure 5.8: Optical spectra (left) with corresponding amplitude fluctuations in the second harmonic (right) for different etalons with a mode separation of $\Delta\lambda$.

mode spacing.

A more detailed description of this experiment can be found in paper V.

6

Conclusion

In this thesis, I have described how new components such as volume Bragg gratings and carbon nanotube doped films can be used to construct compact solid-state lasers in the near infrared spectral range. A number of different lasers have been realized:
In paper I we demonstrated a diode-pumped Yb:KYW laser, where a transversely chirped volume Bragg grating replaces the laser output coupler for spectral control, narrowing and tuning. The wavelength could easily be tuned from 997 nm to 1016 nm by translating the grating, yielding an output power of up to 3.3 W. The laser cavity features a simple and compact design, and this new method of tuning a solid-state laser is generally applicable to many other laser systems, as presented in paper II.
In paper II, a Nd:YVO_4 laser was spectrally locked using a transversally chirped volume Bragg grating to achieve both single-longitudinal-mode output and tuning of the laser around the emission wavelength of 1,064 μm. Inserting a Cr^{4+}:YAG saturable absorber in the linear cavity, Q-switched pulses with a pulse duration of 4 ns and a pulse energy of 5.7 μJ were achieved. In an external frequency-doubling scheme, using periodically-poled KTP for second-harmonic generation, a conversion efficiency exceeding 50 % was demonstrated.
In paper III, an Yb-doped fiber laser was cryogenically cooled in order to increase the efficiency of the laser. The drawback of this method is a reduced reabsorption in combination with a reduced homogeneous broadening, which tends to broaden the output spectrum. A volume Bragg grating was used to overcome this problem by locking and narrowing the spectrum and, at the same time, maintaining a highly efficient laser. We could extract 11.4 W of output power with a spectral bandwidth of less than 0.4 nm at 14.5 W of launched pump light.
In paper IV, an Yb:KYW was fundamentally mode-locked in a 1 GHz cavity employing a semiconductor quantum dot saturable absorber mirror. Without dispersion compensation, the cavity delivered 1.7 ps wide pulses at an average output power of up to 339 mW at wavelengths around 1.032 μm. The output power was limited

by the saturable absorber's damage threshold.
In paper V, large amplitude fluctuations, that can occur in intracavity frequency-doubled lasers, are experimentally described for a semiconductor disk lasers. These lasers typically exhibit stable emission because of their tendency to single-mode operation and the high gain coupling of different modes due to an extremely short gain medium and the resonant periodic gain structure. We demonstrated a dependence of the fluctuation amplitude on gain decoupling of different fundamental modes. This has been done by employing etalons of different thickness for the spectral separation of the longitudinal modes, which couple through sum frequency generation. Using BiBO as the nonlinear crystal for the intracavity frequency doubling, a conversion efficiency of 80 % with respect to the available fundamental power has been achieved.
In paper VI, an Yb:KYW laser was intra-cavity frequency doubled to the green using a periodically-poled Rb:KTP crystal. The the output power exceeded 1 W at 514.7 nm. Spectral narrowing and locking at the fundamental wavelength has been achieved by using a volume Bragg grating as the input coupler. In addition, we presented a detailed analysis on the thermal limitations of the volume Bragg grating.
In paper VII we demonstrated mode-locking of an optically pumped semiconductor disk laser by using a single-walled carbon nanotube saturable absorber in transmission in a simple, V-shaved cavity. Stable passive fundamental mode-locking was obtained at a repetition rate of 613 MHz with a pulse length of 1.23 ps. The laser delivered a maximum average output power of 136 mW at 1074 nm.

6.1 Outlook

The experiments have shown that volume Bragg gratings are well-suited for many practical applications requiring precise spectral control and tuning of a laser. A next natural step towards further improvement and increase in compactness would be an integration of the components. One possibility would be a direct bonding of the volume Bragg grating onto the laser crystal. Another example would be the direct incorporation of carbon nanotubes in the photo-thermo refractive glass in order to eliminate the necessity of a (PMMA-) matrix for the saturable absorbers.

Bibliography

[Abr04] R. H. Abram, K. S. Gardner, E. Riis, and A. I. Ferguson, *Narrow linewidth operation of a tunable optically pumped semiconductor laser,* Opt. Express **12**, 5434-5439 (2004).

[Alf02] W. J. Alford, T. D. Raymond and A. A. Allerman, *High power and good beam quality at 980 nm from a vertical external-cavity surface-emitting laser*, Journal of the Optical Society of America B **19**, 663-666 (2002).

[Arm62] J. A. Armstrong, N. Bloembergen, J. Ducuing and P. S. Pershan, *Interactions between light waves in a nonlinear dielectric*, Physical Review **127**, 1918-1938 (1962).

[Bae86] T. Baer, *Large-amplitude fluctuations due to longitudinal mode coupling in diode-pumped intracavity-doubled Nd:YAG lasers*, Journal of the Optical Society of America B **3**, 1175-1180 (1986).

[Bas62] M. Bass, P. A. Franken, A. E. Hill, C. W. Peters and G. Weinreich, *Optical mixing*, Phys. Rev. Lett. **8**, 18 (1962).

[Ber04] L. Bergmann, C. Schaefer, H. Niedrig, *Lehrbuch der Experimentalphysik Bd.3 Optik*, de Gruyter, Berlin, 10. Auflage (2003).

[Bie89] J. D. Bierlein, H. Vanherzeele, *Potassium titanyl phosphate: properties and new applications*, J. Opt. Soc. Am. B **6**, 622 (1989).

[Bor99] M. Born, E. Wolf, *Principles of Optics, Seventh Edition*, Cambridge University Press, Cambridge (1999).

[Boy68] G. D. Boyd and D. A. Kleinmann, *Parametric Interaction of Focused Gaussian Light Beams,* J. Appl. Phys. **39**, 3597-3639 (1968).

[Boy03] R. W. Boyd, *Nonlinear Optics, Second Edition*, Academic Press, San Diego (2003).

[Bra91] C. Bracikowski and R. Roy, *Chaos in a multimode solid-state laser system*, Chaos: An Interdisciplinary Journal of Nonlinear Science **1**, 49-64 (1991).

[Bre01] A. Brenier, *A new evaluation of Yb^{3+}-doped crystals for laser application*, J. Lumin. **92**, 199-204 (2001).

[But95] S. D. Butterworth, S. Girard, and D. C. Hanna, *High power, broadly tunable all-solid-state synchronously pumped LBO optical parametric oscillator*, J. Opt. Soc. Am. B **12**, 2158 (1995).

[Can05] C. Canalias, *Domain engineering in $KTiOPO_4$*,Dissertation, Royal Institute of Technology, Stockholm, Sweden 2005.

[Che11] K. Cheng, S. Z. Zhao, K. J. Yang, G. Q. Li, D. C. Li, G. Zhang, B. Zhao, and Y. G. Wang, *Diode-pumped passively Q-switched Nd: $Lu_{0.33}\,Y_{0.37}\,Gd_{0.3}\,VO_4$ laser using a single-walled carbon nanotube saturable absorber,* Laser Phys. Lett. **8**, 418-422 (2011).

[Cho08] W. B. Cho, J. H. Yim, S. Y. Choi, S. Lee, U. Griebner, V. Petrov, and F. Rotermund, *Mode-locked self-starting Cr:forsterite laser using a single-walled carbon nanotube saturable absorber,* Opt. Lett. **33**, 2449-2451 (2008).

[Cho10] W. B. Cho, J. H. Yim, S. Y. Choi, S. Lee, A. Schmidt, G. Steinmeyer, U. Griebner, V. Petrov, D.-I. Yeom, K. Kim, and F. Rotermund, *Boosting the nonlinear optical response of carbon nanotube saturable absorbers for broadband mode-locking of bulk lasers,* Adv. Funct. Mater. **20**, 1937-1943 (2010).

[Col63] S. A. Collinds and R.G. White, *Interferometer laser mode selector*, Appl. Opt. **2**, 448 (1963).

[Cze02] C. Czeranowsky, *Resonatorinterne Frequenzverdopplung von diodengepumpten Neodym-Lasern mit hohen Ausgangsleistungen im blauen Spektralbereich*, Dissertation, Institut für Laser-Physik, Universität Hamburg (2002).

[Das96] T. Dascalu, N. Pavel, V. Lupei, G. Philipps, T. Beck, H. Weber, *Investigation of a passive Q-switched, externally controlled, quasicontinuous or continuous pumped Nd:YAG laser ,* Opt. Eng. **35**, 1247-1251 (1996).

[DiD62] J. M. DiDomenico, R. H. Pantell, O. Svelto and J. N. Weaver, *Optical frequency mixing in bulk semiconductors*, Appl. Phys. Lett. **1**, 77 (1962).

[Efi99] O. Efimov, L. Glebov, L. Glebova, K. Richardson, and V. Smirnov, *High-efficiency Bragg gratings in photothermorefractive glass,* Appl. Opt. **38**, 619-627 (1999).

[Efi99b] O. M. Efimov, L. B. Glebov, S. Papernov and A. W. Schmid, *Laser-induced damage of photo-thermo-refractive glasses for optical holographic element writing*, Proc. SPIE **3578**, 564 (1999).

[Ein16] A. Einstein, *Strahlungsemission und -absorption nach der Quantentheorie*, Verhandlungen DPG **318** (1916).

[Ein17] A. Einstein, *Zur Quantentheorie der Strahlung*, Physikalische Zeitschrift **18**, 121 (1917).

[Fej92] M. M. Fejer, G. A. Magel, D. H. Jundt, and R. L. Byer, *Quasi-Phase-Matched Second Harmonic Generation: Tuning and Tolerances,* IEEE J. Quant. Electr. **28**, 2631-2654, (1992).

[Fra61] P. A. Franken, A. E. Hill, C. W. Peters and G. Weinreich, *Generation of optical harmonics*, Phys. Rev. Lett. **7**, 118 (1961).

[Gie94] A. Giesen, H. Hügel, A. Voss, K. Wittig, U. Brauch, and H. Opower, *Scalable concept for diode-pumped high-power solid-state lasers*, Appl. Phys. B **58**, 365-372 (1994).

[Gio62] J. A. Giordmaine, *Mixing of light beams in crystals*, Phys. Rev. Lett. **8**, 19 (1962).

[Gle92] L. B. Glebov, N. V. Nikonorov, E. I. Panysheva, G. T. Petrovski, V. V. Savvin, I. V. Tunimanova and V. A. Tsekhomski, *New ways to use photosen- sitive glasses for recording volume phase holograms*, Opt. Spectrosc. **73**, 237 (1992).

[Gle04] L. B. Glebov, L. N. Glebova, V. I. Smirnov, M. Dubinskii, L. D. Merkle, S. Papernov and A. W. Schmid, *Laser damage resistance of photo-thermo-refractive glass bragg gratings*, Solid-state and diode laser technology review (Albuquerque, USA, June 8-10, 2004).

[Hae02] R. Häring, R. Paschotta, A. Aschwanden, E. Gini, F. Morier-Genoud, and U. Keller, *High-power passively mode-locked semiconductor lasers*, IEEE J. of Quant. Elec.**38**, 1268-1275 (2002).

[Hag07] I. Häggström, B. Jacobsson, and F. Laurell, *Monolithic Bragg-locked Nd:$GdVO_4$ laser,* Opt. Express **15**, 11589-11594 (2007).

[Hal62] R. N. Hall, G. E. Fenner, J. D. Kingsley, T. J. Soltys and R. O. Carlson, *Coherent light emission from GaAs junctions*, Phys. Rev. Letter **9**, 366-368 (1962).

[Har07] R. Hartke, E. Heumann, G. Huber, M. Kühnelt, U. Steegmüller, *Efficient green generation by intracavity frequency doubling of an optically pumped semiconductor disk laser.*, Appl. Phys. B **87**, 95-99 (2007).

[Hau75] H. A. Haus, *Theory of mode locking with a fast saturable absorber*, J. of Appl. Phys. **46**, 3049 (1975).

[Hau00] H. A. Haus, *Mode-locking of lasers*, IEEE J. Select. Topics Quantum Electron. **6**, 1173 (2000).

[Hec98] E. Hecht, *Optics, Third Edition*, Addison-Wesley, New York (1998).

[Hel94] S.W. Hell, J. Wichmann, *Breaking the diffraction resolution limit by stimulated emission: stimulated-emission-depletion fluorescence microscopy,* Opt. Lett. **19**, 780-782 (1994).

[Hel06] J. E. Hellström, S. Bjurshagen, V. Pasiskevicius, J. Liu, V. Petrov, and U. Griebner, *Efficient Yb:KGW lasers end-pumped by high-power diode bars,* Appl. Phys. B **bf 83**, 235-239 (2006).

[Hel07] J. E. Hellström, B. Jacobsson, V. Pasiskevicius, and F. Laurell, *Quasi-two-level Yb:KYW laser with a volume Bragg grating,* Opt. Express **15**, 13930-13935 (2007).

[Hel08] J. E. Hellström, B. Jacobsson, V. Pasiskevicius, and F. Laurell, *Finite beams in reflective volume Bragg gratings: theory and experiments,* IEE J. Quant. Elec. **44**, 81 (2008).

[Hen89] B. Henderson and G.F. Imbusch, *Optical spectroscopy of inorganic solids*, Clarendon Press (1989).

[Hen07] M. Henriksson, L. Sjöqvist, V. Pasiskevicius, and F. Laurell, *Narrow linewidth 2 μm OPO in periodically poled $LiNbO_3$ with volume Bragg grating output coupler*, Appl. Phys. B **86**, 497-501 (2007).

[Hen09] M. Henriksson, L. Sjöqvist, V. Pasiskevicius, and F. Laurell, *Spectrum of multi-longitudinal mode pumped near-degenerate OPOs with volume Bragg grating output couplers*, Opt. Express **17**, 17582-17589 (2009).

[Hoe99] C. Hönninger, R. Paschotta, F. Morier-Genoud, M. Moser, and U. Keller, *Q-switching stability limits of cw passive mode locking*, J. Opt. Soc. Am. B **16**, 46 (1999).

[Hof11] M. Hoffmann, O. D. Sieber, V. J. Wittwer, I. L. Krestnikov, D. A. Livshits, Y. Barbarin, T. Südmeyer, U. Keller, *Femtosecond high-power quantum dot vertical external cavity surface emitting laser*, Opt. Express **19**, 8108 (2011).

[Hub10] G. Huber, C. Kränkel, and K. Petermann, *Solid-state lasers: status and future*, J. Opt. Soc. Am. B **27**, B93 (2010).

[Iij91] S. Iijima, *Helical microtubules of graphitic carbon*, Nature **354**, 56 (1991).

[Jac05] B. Jacobsson, M.Tiihonen, V. Pasiskevicius, and F. Laurell, *Narrowband bulk Bragg grating optical parametric oscillator*, Opt. Letters **30**, 2281 (2005).

[Jac06] B. Jacobsson, V. Pasiskevicius, and F. Laurell, *Tunable single-longitudinal-mode ErYb:glass laser locked by a bulk glass Bragg grating,* Opt. Letters **31**, 1663-1663 (2006).

[Jac07a] B. Jacobsson, V. Pasiskevicius, and F. Laurell, *Single-longitudinal Nd-laser with a Bragg-grating Fabry-Perot cavity,* Opt. Express **14**, 9284-9292 (2007).

[Jac07b] B. Jacobsson, J. E. Hellström, V. Pasiskevicius, and F. Laurell, *Widely tunable Yb:KYW laser with a volume Bragg grating,* Opt. Express **15**, 1003-1010 (2007).

[Jac08a] B. Jacobsson, J. E. Hellström, V. Pasiskevicius, F. Laurell, *Tunable Yb:KYW laser using volume Bragg grating in s-polarization,* Appl. Phys. B **91**, 85-88 (2008).

[Jac08b] B. Jacobsson, *Experimental and theoretical investigations of a volume-Bragg-grating-locked Yb:KYW laser at selected wavelengths,* Opt. Express **16**, 6443-6454 (2008).

[Jel07a] P. Jelger and F. Laurell, *Efficient narrow-linewidth VBG-locked Nd:fiber laser*, Opt. Express **15**, 11336-11340 (2007).

[Jel07b] P. Jelger and F. Laurell, *Efficient skew-angle cladding-pumped tunable narrow-linewidth Yb-doped fiber laser*, Opt. Lett. **32**, 3501-3503 (2007).

[Jel09] P. Jelger, *High performance fiber lasers with spectral, thermal and lifetime control,*Dissertation, Royal Institute of Technology, Stockholm, Sweden 2009.

[Jel10] P. Jelger, V. Pasiskevicius, and F. Laurell, *Narrow linewidth high output coupling dual VBG-locked Yb-doped fiber-laser*, Opt. Express **18**, 980-4980 (2010).

[Jam90] G. E. James, E. M. Harrell, II and R. Roy *Intermittency and chaos in intracavity doubled lasers. II*, Phys. Rev. A **41**, 2778-2790 (1990).

[Jim08] J. H. Yim, W. B. Cho, S. Lee, Y. H. Ahn, K. Kim, H. Lim, G. Steinmeyer, V. Petrov, U. Griebner, and F. Rotermund, *Fabrication and characterization of ultrafast carbon nanotube saturable absorbers for solid-state laser mode-locking near 1 μm,* Appl. Phys. Lett. **93**, 161106 (2008).

[Kae98] F. X. Kärtner, J. Aus der Au, and U. Keller, *Mode-locking with slow and fast saturable absorbers – what's the difference?*, IEEE J. Sel. Topics in Quantum Electr. **4**, 159 (1998).

[Kae04] F. X. Kärtner (Ed.), *Few-Cycle Laser Pulse Generation and Its Applications*, Springer (2004).

[Kel06] U. Keller, A. C. Tropper, *Passively modelocked surface-emitting semiconductor lasers*, Physics Report **429**, 67-120 (2006).

[Key64] R. J. Keyes and T. M. Quist, Injection luminescent pumping of CaF_2:U^{3+} with GaAs diode lasers, Appl. Phys. Lett. **4**, 50 (1964).

[Kim08] J. W. Kim, P. Jelger, J. K. Sahu, F. Laurell, and W. A. Clarkson, *Narrow linewidth high output coupling dual VBG-lcoked Yb-doped fiber-laser*, Opt. Lett. **33**, 1204-1206 (2008).

[Koe06] W. Koechner, *Solid-state laser engineering*, Springer, (2006).

[Kra92] F. Krausz, M. E. Fermann, T. Brabec, P. F. Curley, M. Hofer, M. H. Ober, C. Spielmann, E. Wintner, and A. J. Schmidt, *Femtosecond solid-state lasers*, IEEE J. of Quantum Electronics (1992), **28**, 2097 (1992).

[Kuz97] M. Kuznetsov, F. Hakimi, R. Sprague and A. Mooradian, *High power (>0,5 W cw) diode-pumped vertical-external-cavity surface-emitting semiconductor lasers with circular TEM00 beams*, IEEE Photonics Technology Letters **9**, 1063-1065 (1997).

[Li06] W. Li, Q. Hao, H. Zhai, H. Zeng, W. Lu, G. Zhao, C. Yan, L. Su and J. Xu, *Low-threshold and continuously tunable Yb:Gd_2SiO_5 laser*, Appl. Phys. Lett. **89**, 101125 (2006).

[Li12] C. Y. Li, Y. Bo, N. Zong, Y. G. Wang, B. X. Jiang, Y. B. Pan, G. Niu, Z. W. Fan, Q. J. Peng, D. F. Cui, Z. Y. Xu, *LD-end-pumped passively Q-switched Nd:YAG ceramic laser with single wall carbon nanotube saturable absorber,* Opt. and Laser Techn. **44**, 2149-2153 (2012).

[Lin96] G. Lindström und R.Langkau, *Physik kompakt: Quantenphysik*, Vieweg Verlag (1996).

[Liu05] J. Liu, U. Griebner, V. Petrov, H. Zhang, J. Zhang, and J. Wang, *Efficient continuous-wave and Q-switched operation of a diode-pumped Yb:$KLu(WO_4)_2$ laser with self-Raman conversion,* Opt. Lett. **30**, 2427-2429 (2005).

[Lut03] S. Lutgen, T. Albrecht, P. Brick, W. Reill, J. Luft, and W. Spath, *8-W high-efficiency continuous-wave semiconductor disk laser at 1000 nm*, Applied Physics Letters **82**, 3620-3622 (2003).

[Mag93] V. Magni, G. Cerullo, S. De Silvestri, 0. Svelto, L. J. Qian, and M. Danailo, *Intracavity frequency doubling of a cw high-power TEM_{00} Nd:YLF laser* Opt. Letters, **18**, 2111-2113 (1993).

[Mai60] T. H. Maiman, *Stimulated optical radiation in ruby*, Nature **187**, 493 (1960).

[Mak62] P. D. Maker, R. W. Terhune, M. Nisenoff and C. M. Savage, *Effects of dispersion and focusing on the production of optical harmonics*, Phys. Rev. Lett. **8**, 21 (1962).

[Mar84] O. E. Martinez, R. L. Fork, and J. P. Gordon, *Theory of passively mode-locked lasers including self-phase modulation and group-velocity dispersion*, Opt. Lett. **9**, 156 (1984).

[Mcc62] F. J. McClung and R. W. Hellwarth, *Giant optical pulsations from ruby*, J. Appl. Phys. **33**, 828 (1962).

[Mes90] A. Messiah, *Quantenmechanik, Volume 2*, Verlag de Gruyter, 828 (1990).

[Moe66] G. Moeller and J. D. Rigden, *Observation of laser action in the R-branch of CO_2 and N_2O vibrational spectra*, Appl. Phys. Lett. **8**, 69 (1966).

[Nat62] M. I. Nathan, W. P. Dumke, G. Burns, F. H. Dill, Jr., and G. J. Lasher, *Stimulated emission of radiation from GaAs p-n junctions*, Applied Physics Letters **1**, 62 (1962).

[Pas01] V. Pasiskevicius, H. Karlsson, F. Laurell, R. Butkus, V. Smilgevicius, and A. Piskarskas, *High-efficiency parametric oscillation and spectral control in the red spectral region with periodically poled $KTiOPO_4$,* Opt. Letters, **26**, 710-712 (2001).

[Pei04] H.-O. Peitgen, H. Jürgens, D. Saupe, *Chaos and Fractals*, Springer Verlag, Berlin (1999).

[Pet07] R. Peters, C. Kränkel, K. Petermann, and G. Huber, *Broadly tunable high-power Yb:Lu_2O_3 thin disk laser with 80 % slope efficiency*, Opt. Express **15**, 7075-7082 (2007).

[Pow98] R.C. Powell, *Physics of solid-state laser materials*, AIP Press and Springer, (1998).

[Qin11] H. Qin, Z. Zhuo, J. Liu, H. Zhang, Y. Wang, *Diode pumped passively Q-switched Nd:YVO_4 laser with a carbon nanotube saturable absorber*, Laser Phys. **21**, 1562-1565 (2011).

[Ris03] W. P. Risk, T. R. Gosnell, A.V. Nurmikko, *Compact Blue-Green Lasers* (Cambridge University Press, 2003).

[Rot12] F. Rotermund, W. B. Cho, S. Y. Choi, I. H. Baek, J. H. Yim, S. Lee, A. Schmidt, G. Steinmeyer, U. Griebner, D.-I. Yeom, K. Kim, and V. Petrov, M*ode-locking of solid-state lasers by single-walled carbin-nanotube based saturable absorbers*, Quantum Electron. **42**, 663 (2012).

[Qui62] T. M. Quist, R. H. Rediker, R. J. Keyes, W. E. Krag, B. Lax, A. L. McWorther and H. J. Zeigler, *Semiconductor maser of GaAs*, Physical Review Letter **9**, 91-92 (1962).

[San06] S. Santran, M. Martinez-Rosas, L. Canioni, L. Sarger, L. N. Glebova, A. Tirpak and L. B. Glebov, *Nonlinear refractive index of photo-thermo-refractive glass*, Opt. Mater. **28**, 401 (2006).

[Sch58] A. L. Schawlow and C.H. Townes, *Infrared and optical masers*, Physical Review **112**, 1940 (1958).

[Sch09] A. Schmidt, S. Rivier, W. B. Cho, J. H. Yim, S. Y. Choi, S. Lee, F. Rotermund, D. Rytz, G. Steinmeyer, V. Petrov, and U. Griebner, *Sub-100 fs single-walled carbon nanotube saturable absorber mode-locked Yb-laser operation near 1 μm,* Opt. Express, **17**, 20109-20116 (2009).

[Set04] S. Y. Set, H. Yaguchi, Y. Tanaka, and M. Jablonski, *Laser mode locking using a saturable absorber incorporating carbon nanotubes,* J. Lightwave Techn. **22**, 51-56 (2004).

[She95] C. J. R. Sheppard, *Approximate calculation of the reflection coefficient from a stratified medium*, Pure Appl. Opt. **4**, 665 (1995).

[Shi95] Y. Shimony, Z. Burshtein, Y. Kalisky, *Repetitive Q-switching of a CW Nd:YAG laser using Cr^{4+}:YAG saturable absorbers,* IEEE J. Quantum Electron. **31**, 1738 (1995).

[Sie86] A. Siegman, *Lasers*, University Science Books, Sausalito, California (1986).

[Sla29] J. Slater, H. C. Verma, *The Theory of Complex Spectra*, Phys. Rev. **34**, 1293 (1929).

[Sut96] R. L. Sutherland, *Handbook of nonlinear optics*, Marcel Dekker, Inc., New York (1996).

[Sve89] O. Svelto, *Principles of Lasers, Third Edition*, Plenum Press, New York and London (1989).

[Sza89] A. Szabo, N. S. Ostlund, *Modern Quantum Chemistry: Introduction to Advanced Electronic Structure Theory*, McGraw-Hill, New York (1989).

[Tow03] C. H. Townes, *The first laser*, A Century of Nature: Twenty-One Discoveries that Changed Science and the World, University of Chicago Press (2003).

[Tro04] A. C. Tropper, H. D. Foreman, A. Garnache, K. G. Wilcox, and S. H. Hoogland, *Vertical-external-cavity semiconductor lasers*, J. Phys. D: Appl. Phys. **37**, R75-R85 (2004).

[Tro06] A. C. Tropper, S. H. Hoogland, *Extended cavity surface-emitting semiconductor lasers*, Progress in Quantum Electronics **30**, 1-43 (2006).

[Van92] H. Vanherzeele and J. D. Bierlein, *Magnitude of the nonlinear-optical coefficients of $KTiOPO_4$*, Opt. Lett. **17**, 982 (1992).

[Ven05] G. B. Venus, A. Sevian, V. I. Smirnov and L. B. Glebov, *High-brightness narrow-line laser diode source with volume Bragg-grating feedback*, Proc. SPIE **5711**, 166 (2005).

[Wan05] S. Wang, *Fabrication and characterization of periodically-poled KTP and Rb-doped KTP for applications in the visible and UV*, Dissertation, Royal Institute of Technology, Stockholm, Sweden 2005.

[Wan07] S. Wang, V. Pasiskevicius, and F. Laurell, *High-efficiency frequency converters with periodically-poled Rbdoped $KTiOPO_4$,* Opt. Mater. **30**, 594-599 (2007).

[Wit12] V. J. Wittwer, M. Mangold, M. Hoffmann, O. D. Sieber, M. Golling, T. Südmeyer, U. Keller, *High-power integrated ultrafast semiconductor disk laser: multi-Watt 10 GHz pulse generation*, Electron. Lett. **48**, 1144 (2012).

[Wu87] X.-G. Wu and P. Mandel, *Second-harmonic generation in a multimode laser cavity*, Journal of the Optical Society of America B **4**, 1870-1877 (1987).

[Xia97] G. Xiao, M. Bass, *A generalized model for passively Q-switched lasers including excited state absorption in the saturable absorber,* IEEE J. Quantum Electron. **33**, 41-44 (1997).

[Yar89] A. Yariv, *Quantum electronics 3^{rd} ed.*(Wiley, New York,1989).

[Yim08] J. H. Yim, W. B. Cho, S. Lee, Y. H. Ahn, K. Kim, H. Lim, G. Steinmeyer, V. Petrov, U. Griebner, and F. Rotermund, *Fabrication and characterization of ultrafast carbon nanotube saturable absorbers for solid-state laser mode-locking near 1 μm*, Appl. Phys. Lett. **93**, 161106 (2008).

[Zha97] X. Zhang, S. Zhao, Q. Wang, Q. Zhang, L. Sun, S. Zhang, *Optimization of Cr^{4+}-doped saturable-absorber Qswitched lasers*, IEEE J. Quantum Electron. **33**, 2286 (1997).

[Zuk13] A. Zukauskas, V. Pasiskevicius and C. Canalias, *Second-harmonic generation in periodically poled bulk Rb-doped $KTiOPO_4$ below 400 nm at high peak-intensities,* Opt. Express **21**, 1395-1395 (2013).

[Zwa06] J. W. Zwanziger, U. Werner, E. D. Zanotto, E. Rotari, L. N. Glebova, L. B. Glebov and J. F. Schneider, *Residual internal stress in partially crystallized photothermorefractive glass: Evaluation by nuclear magnetic resonance spectroscopy and ?rst principles calculations*, J. Appl. Phys. **99**, 083511 (2006).

Part II

Papers I - VII

Paper I

Kai Seger, Björn Jacobsson,
Valdas Pasiskevicius and Fredrik Laurell

Tunable Yb:KYW laser using a
transversely chirped volume Bragg grating

Optics Express **17**, 2341 (2009).

Paper II

Kai Seger, Niels Meiser, Carlota Canalias
Valdas Pasiskevicius and Fredrik Laurell

Tunable, passively Q-switched single-longitudinal-mode Nd:YVO_4 laser using a chirped volume Bragg grating

Applied Physics B **109**, 99 (2012).

Paper III

Pär Jelger, Kai Seger,
Valdas Pasiskevicius and Fredrik Laurell

Highly efficient temporally stable narrow linewidth cryogenically cooled Yb-fiber laser

Optics Express **17**, 8433 (2009).

Paper IV

Niels Meiser, Kai Seger, Valdas Pasiskevicius,
Hoon Jang, Edik Rafailov and Igor Krestnikov

GHz repetition rate mode-locked Yb:KYW laser
using self-assembled quantum dot saturable absorber

Applied Physics B **110**, 327 (2013).

Paper V

Rene Hartke, Valery Baev, Kai Seger, Oliver Back
Ernst Heumann, Günter Huber, Michael Kühnelt,
Ulrich Steegmüller

Experimental study of the output dynamics of
intracavity frequency doubled OPSDL

Applied Physics Letters **92**, 101107 (2008).

Paper VI

Kai Seger, Niels Meiser, Staffan Tjörnhammar
Andrius Zukauskas, Carlota Canalias, Valdas Pasiskevicius and Fredrik Laurell

Intra-cavity frequency-doubled Yb:KYW laser using periodically poled Rb-doped KTP with a volume Bragg grating input coupler

Submitted for publication (2013).

Paper VII

Kai Seger, Niels Meiser, Sun Young Choi, Bo Hee Jung, Dong-Il Yeom, Fabian Rotermund, Oleg Okhotnikov, Fredrik Laurell and Valdas Pasiskevicius

Carbon nanotube mode-locked optically-pumped semiconductor disk laser

Submitted for publication (2013).